[18] K. Okabe, X. Li, M. Wei, H. Arakwa, Catal. Today 89 (2004) 431.
[19] R.B. Anderson, The Fischer–Tropsch Synthesis, Academic Press, San Diego, 1984.
[20] D. Schanke, S. Vada, E.A. Blekkan, A. Hilmen, A. Hoff, A. Holmen, J. Catal. 156 (1995) 85.
[21] Y. Zhang, D. Wei, S. Hammache, J.G. Goodwin Jr., J. Catal. 188 (1999) 281.
[22] A. Lapidus, A. Krylova, V. Kazanskii, Z. Borovkov, J. Ratnousky, A. Zukal, M.C. Jan, Appl. Catal. A 186 (1999) 145.
[23] J. Panpranot, J.G. Goodwin Jr., A. Sayari, Catal. Today 77 (2002) 269.
[24] A.M. Hilmen, D. Schanke, A. Holmen, Catal. Lett. 38 (1996) 143.
[25] A. Lapidus, A. Krylova, V. Kazanskii, Z. Borovkov, A. Zaitsev, Appl. Catal. A 73 (1991) 65.

Available online at www.sciencedirect.com

SCIENCE DIRECT

Materials Letters 59 (2005) 3771 – 3774

materials letters

www.elsevier.com/locate/matlet

Impact of diene addition on properties for ethylene–propylene copolymerization with *rac*-Et[Ind]$_2$ZrCl$_2$/MAO catalyst

Bunjerd Jongsomjit [a,*], Sireethorn Phoowakeereewiwat [a], Supakanok Thongyai [a], Takeshi Shiono [b], Piyasan Praserthdam [a]

[a] *Center of Excellence on Catalysis and Catalytic Reaction Engineering, Department of Chemical Engineering, Faculty of Engineering, Chulalongkorn University, Bangkok 10330, Thailand*

[b] *Department of Applied Chemistry, Faculty of Engineering, Hiroshima University, Higashi-Hiroshima 739-8527, Japan*

Received 20 May 2005; accepted 7 July 2005
Available online 28 July 2005

Abstract

In the present study, the impact of diene addition during copolymerization of ethylene and propylene using a metallocene/MAO catalyst was investigated. It showed that with a small amount of diene added, the dienes (except for ENB) did not incorporate in the polymer backbone pronouncedly. However, the addition of dienes can alter the incorporation of ethylene and propylene in the polymer backbone according to different types of dienes used. The catalytic behaviors and yields were not significant changes with the addition of dienes. The characteristics of polymer obtained using ^{13}C NMR, SEM, and DSC were also further discussed in more detail.

Keywords: Polymerization; Metallocene; Catalyst; Elastomers; Methylaluminoxane

1. Introduction

It is known that the copolymerization of ethylene (E) and propylene (P) can result in a production of rubbery materials called EP elastomers [1–3]. Because there are no double bonds in the backbone of polymer chain, they are usually insensitive to oxygen, ozone, acids, and alkaline. It was found that addition of the third monomer such as dienes could be applied in order to escalate the properties of EP elastomers, the so-called EPDM elastomers. As known, EPDM can be widely used in many applications so far [4–6]. Currently, EPDM is synthesized using vanadium-based catalysts. With the presence of dienes, it was found that the vanadium-based catalysts exhibited low activities along with toxicity concerns due to the residual vanadium remains in the polymer [7]. Thus, in order to overcome those problems, an alternative way of using the homogeneous metallocene catalysts has been substantially investigated by many authors [8–10]. Nevertheless, the production of EPDM is considered to be an important matter, the approach of our present study was apparently different from the

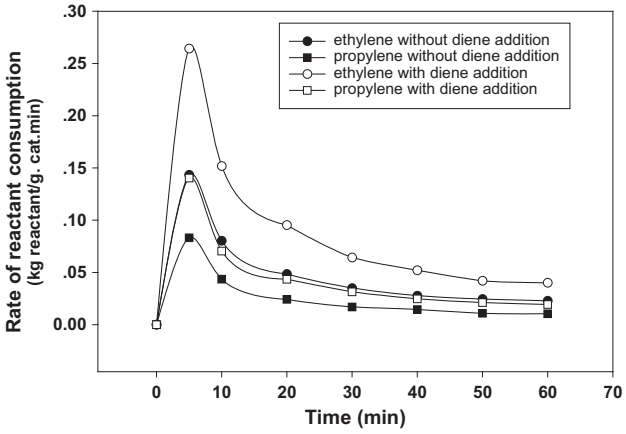

Fig. 1. Activity profiles based on ethylene (E) and propylene (P) consumption with and without diene addition.

* Corresponding author. Tel.: +66 662 2186869; fax: +66 662 2186877.
E-mail address: bunjerd.j@chula.ac.th (B. Jongsomjit).

0167-577X/$ - see front matter © 2005 Elsevier B.V. All rights reserved.
doi:10.1016/j.matlet.2005.07.014

Table 1
Yields and activities of EP elastomers produced from *rac*-Et[Ind]$_2$ZrCl$_2$/MAO catalyst; [Zr]=30 μM in toluene, [Al]/[Zr]=2000, [diene]=0.1 M, E/P molar ratio=75/25, polymerization temperature=40 °C, and polymerization time=1 h

Sample	Types of diene	Polymer yield (g)	Activity (kg polymer/mol Zr h)
EP (0)	None added	2.88	3198
EP(1)	ENB	2.40	2671
EP(2)	VCH	2.60	2887
EP(3)	HD	2.54	2824

others. Hereby, only a small amount of various dienes was introduced into the system during EP copolymerization, not for the purpose of synthesizing the EPDM as in general, but specifically for altering the behaviors of EP copolymerization. Thus, in our present study, the small amount of various dienes added did not incorporate into the polymer backbone, which can be determined using ^{13}C NMR measurement.

2. Experimental

In this study, EP copolymerization was performed using *rac*-Et[Ind]$_2$ZrCl$_2$ catalyst. All chemicals were manipulated under purified argon using a vacuum atmosphere glove boxes and/or Schlenk techniques. Polymerization was carried out in 100-ml stainless steel reactor with magnetic stirrer. First, 30 ml of toluene used as a solvent was added to the reactor. Then, methylaluminoxane (MAO) solution was added according to the specified ratio to the catalyst concentration ([Al]/[Zr]=2000) followed by the addition of 0.1 M of a selected diene [dienes used were 5-ethylidene-2-norbonene (ENB);(1), 4-vinylcyclohexene (VCH);(2), and 1,4-hexadiene (HD);(3)]. Then, the catalyst was injected into the system. The reactor was immediately put into liquid nitrogen to stop the reaction between the catalyst and cocatalyst (MAO). After the reaction mixture was frozen

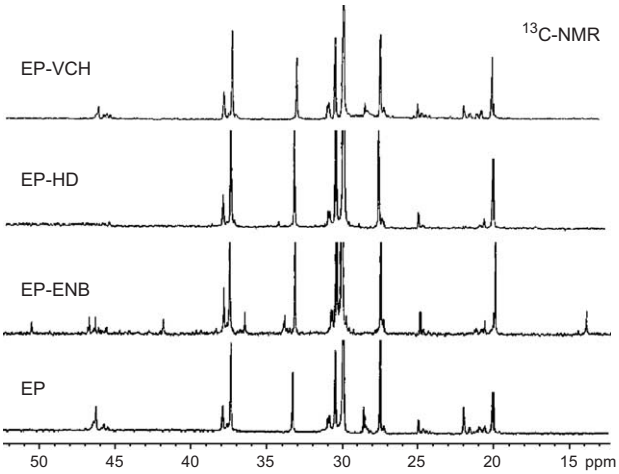

Fig. 2. ^{13}C NMR spectra of various EP elastomers with and without diene addition.

Table 2
Triad distribution obtained by ^{13}C NMR measurement of ethylene (E) and propylene (P) in polymers produced

Sample	Types of diene	EEE	PEE+EEP	PEP	EPE	EPP+PPE	PPP
EP (0)	None added	0.502	0.187	0.045	0.122	0.032	0.112
EP (1)	ENB	0.604	0.191	0.023	0.107	0.024	0.051
EP (2)	VCH	0.505	0.205	0.056	0.114	0.088	0.032
EP (3)	HD	0.609	0.210	0.032	0.118	0.031	–

for 15 min, the reactor was evacuated for 3 min to remove argon then filled with the gaseous monomers (ethylene/propylene with a molar ratio of 75/25) while the reactor was still frozen in liquid nitrogen. Then, the reactor was taken out of liquid nitrogen and heated up to polymerization temperature (40 °C) to start the polymerization reaction. The polymerization time was kept for 1 h. In order to stop the reaction, the gaseous monomers were released and the reaction mixture was washed with acidic methanol. The polymer (white rubbery powder) obtained was filtered and dried overnight at ambient condition. Technically, for each diene, the polymerization was run at least three times to ensure the results obtained. The average values were reported. Characterization of the polymer obtained was performed using the ^{13}carbon nuclear magnetic resonance, ^{13}C NMR (JEOL JMR-A500 operating at 125 MHz), differential scanning calorimetry, DSC (Perkin-Elmer DSC 7), and scanning electron microscopy, SEM (JSM-5800 LV).

3. Results and discussion

The present research indicated that a small amount of dienes (ENB, VCH, and HD) added could have impact on behaviors of ethylene–propylene (EP) copolymerization with a metallocene/MAO catalyst. In fact, a large amount of diene addition could result in a decreased activity of polymerization as reported by Malmberg et al. [5]. However, it should be noted that the large amounts (~10–16 mol%) of diene were technically required in order to produce the terpolymer of EPDM. In particular, only a small amount (~3.6 mol%) of each diene was added during EP copolymerization in this study in order to maintain high activity of polymerization at this specified condition.

The rates of consumption for E and P with and without the diene addition are shown in Fig. 1. It was found that the

Table 3
Incorporation of ethylene (E), propylene (P) and reactivity ratios of ethylene (r_E) and propylene (r_P) calculated from ^{13}C NMR measurement

Sample	Types of diene	Incorporation (%)		Reactivity ratios		
		E	P	r_E	r_P	$r_E r_P$
EP (0)	None added	73	27	5.3	1.9	10.1
EP (1)	ENB[a]	80	18	6.9	1.5	10.4
EP (2)	VCH	76	24	4.8	1.5	7.2
EP (3)	HD	85	15	6.2	1.1	6.8

[a] ENB incorporation ca. 2%.

Table 4
Thermal properties of polymers obtained from DSC measurement

Sample	Types of diene	T_c (°C)	T_m (°C)	ΔH_m (J/g)	% Crystallinity (% χ)
EP (0)	None added	59.3	73.6	30.6	10.6
EP (1)	ENB	57.2	73.8	23.8	8.2
EP (2)	VCH	65.2	80.5	36.3	12.5
EP (3)	HD	70.0	88.2	49.1	17.0

induction period of the catalyst was also observed at the beginning of polymerization. The consumption rate went to a maximum after 6–7 min, then decreased due to catalyst deactivation. With the diene addition, similar activity profiles can still be observed as also shown in Fig. 1. It was suggested that the addition of dienes would have no effect on the catalyst performance at all indicating the similar rate profiles. Yields and activities of various EP elastomers are shown in Table 1. It indicated that the addition of dienes could result in only slightly decreased activities regardless of the dienes used. The polymers obtained were then further characterized using ^{13}C NMR, SEM, and DSC as mentioned. As known, ^{13}C NMR is one of the most powerful techniques used to identify the microstructure of a polymer. The ^{13}C NMR spectra for all polymer samples are shown in Fig. 2. It can be observed that the ^{13}C NMR spectra of EP, EP-VCH, and EP-HD samples exhibited similar patterns corresponding with those as reported by Randall [11]. These revealed that there was no incorporation of HD and VCH in the polymer backbone. The ^{13}C NMR spectrum of EP-ENB sample is also shown in Fig. 2, which apparently exhibited the slightly different patterns compared with other samples as mentioned before. Besides the characteristic peaks of EP copolymer, the incorporation of ENB can be additionally observed at $\delta = 14$, 36.5 and 42 ppm. This indicated that only ENB was able to incorporate into the polymer backbone at this specified condition. The triad distribution, % incorporation, and the reactivity ratios of E and P can be also calculated based on the method described by Randall [11]. The triad distribution of E and P for all samples is shown in Table 2. It indicated that the similar triad distribution was observed, except no block PPP in EP (3) sample. However, % incorporation of E and P along with the reactivity ratios (r_E and r_P) are shown in Table 3. It revealed that upon the addition of a small amount of dienes during copolymerization of EP, the incorporation of ethylene in the polymer apparently increased, especially for the ENB and HD. Since the reactivity ratio of $r_E r_P > 1$, the blocky incorporation of comonomer was obtained, which was different from the behaviors for copolymerization of ethylene and higher 1-olefins such as 1-hexene, 1-octene, and 1-decene [9,10]. The thermal properties such as T_c and T_m obtained from DSC measurement along with % crystallinity [12] are also summarized in Table 4. It was found that T_m, T_c and % crystallinity of EP tended to increase with the addition of dienes. In addition, the various dienes gave different impacts on % crystallinity of EP. It showed that using HD would result in the largest number of T_m, T_c and % crystallinity. The SEM micrographs of various EP produced are shown in Fig. 3. It can be observed that there were some differences in morphologies of the various EP produced. Apparently, the EP produced with the addition of dienes appeared in a larger air gap in the texture compared to those without diene addition. It should be noted that the impact of diene on the different ratios of E/P would be interesting to

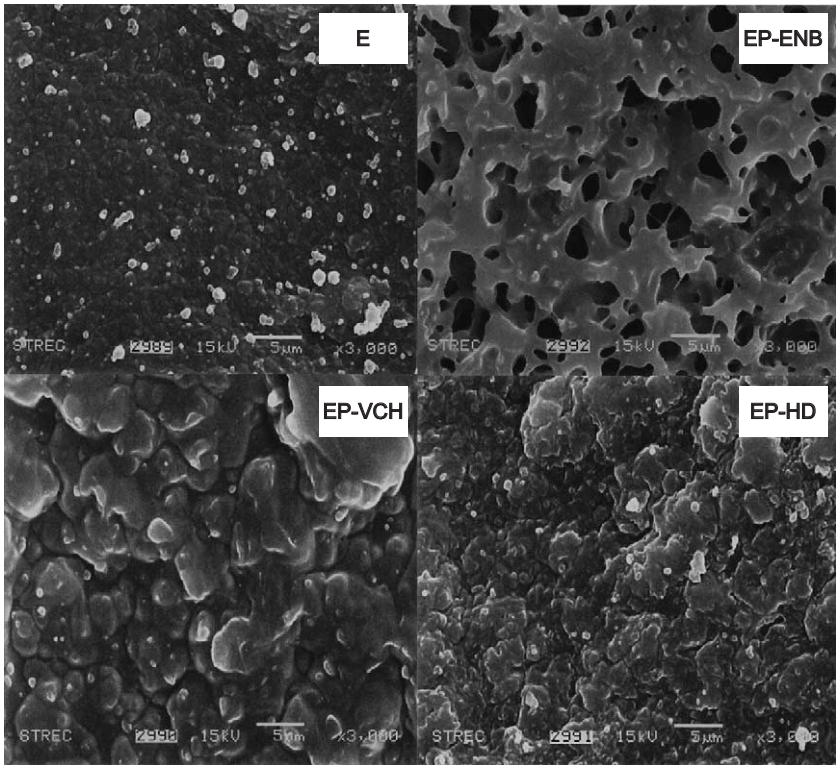

Fig. 3. SEM micrographs of various EP elastomers.

further investigate for our future work. In particular, the various ratios of E/P in the polymer backbone are considered to be the key role to obtain different properties for EP rubbers.

According to our experimental data, the mechanism of this copolymerization of ethylene and propylene could be drawn based on changes in the incorporation of ethylene and propylene upon the diene addition. As seen in Table 3, it can be observed that the insertion of propylene apparently decreased with the diene addition. Therefore, it can be proposed that the addition of diene probably inhibited the propylene insertion catalytic site and/or somehow promoted the catalytic site of ethylene insertion. Those phenomena resulted in a decreased propylene insertion. However, in order to provide a better understanding of the rigorous mechanism inside, we believe that a more powerful technique such as the steady-state isotopic transient kinetic analysis (SSITKA) [13–15], where the reaction intermediates can be identified would be helpful. This technique requires an additional instrument such as a mass spectrometer along with the isotopes (^{13}C) of the corresponding reactants.

4. Conclusions

In summary, our present study revealed, for the first time, that the addition of only a small amount of dienes under the specified condition could alter the copolymerization behaviors of ethylene and propylene instead of making the EPDM as in general. At the specified condition, dienes (except for ENB) did not incorporate into the polymer backbone as proved by ^{13}C NMR. Upon the various dienes used, % incorporation, T_m, T_c, and % crystallinity can be changed dramatically. However, in order to provide a better understanding, the roles of dienes should be further investigated in more detail, especially when the ratios of E/P are varied.

Acknowledgements

The authors thank the Thailand Research Fund (TRF), the National Research Council of Thailand (NRCT), the National Science and Technology Development Agency (NSTDA) and Thailand–Japan Technology Transfer Project (TJTTP-JBIC) for the financial support of this work.

References

[1] W. Kaminsky, M. Miri, J. Polym. Sci., Polym. Chem. 23 (1985) 2151.
[2] R.D. Allen, J. Elastomers Plast. 15 (1983) 19.
[3] E.L. Borg, in: M. Morton (Ed.), Rubber Technology, Krieger, Malabar, FL, 1981, p. 220.
[4] G.V. Strate, in: H.F. Mark, N.M. Bikales, C.G. Overberger, J.J Koschwitz (Eds.), Encyclopedia of Polymer Science and Engineering, J. Wiley & Sons, New York, 1973, p. 522.
[5] A. Malmberg, B. Lofgren, J. Appl. Polym. Sci. 66 (1997) 35.
[6] A. Deffieux, M. Dolakthani, H. Cramail, Macromol. Chem. Phys. 197 (1996) 289.
[7] K.L. Walton, M.M. Hughes, D.R. Parikh, Rubber Chem. Technol. 74 (2001) 688.
[8] W. Kaminsky, A. Laban, Appl. Catal., A Gen. 222 (2001) 47.
[9] B. Jongsomjit, P. Praserthdam, P. Kaewkrajang, Mater. Chem. Phys. 86 (2004) 243.
[10] B. Jongsomjit, P. Kaewkrajang, S.E. Wanke, P. Praserthdam, Catal. Lett. 94 (2004) 205.
[11] C. Randall, Macromol. Chem. Phys. 29 (1989) 201.
[12] S. Ottani, R.S. Porter, J. Polym. Sci., Part B, Polym. Phys. 29 (1991) 1179.
[13] A.R. Belambe, R. Oukaci, J.G. Goodwin Jr., J. Catal. 166 (1997) 8.
[14] S.L. Shannon, J.G. Goodwin Jr., Chem. Rev. 95 (1995) 677.
[15] B. Jongsomjit, J. Panpranot, J.G. Goodwin Jr., J. Catal. 215 (2003) 66.

Available online at www.sciencedirect.com
SCIENCE DIRECT®
Catalysis Communications 6 (2005) 705–710
CATALYSIS COMMUNICATIONS
www.elsevier.com/locate/catcom

Characteristics and catalytic properties of Co/TiO_2 for various rutile:anatase ratios

Bunjerd Jongsomjit *, Tipnapa Wongsalee, Piyasan Praserthdam

Center of Excellence on Catalysis and Catalytic Reaction Engineering, Department of Chemical Engineering, Faculty of Engineering, Chulalongkorn University, Bangkok 10330, Thailand

Received 21 March 2005; received in revised form 5 July 2005; accepted 5 July 2005
Available online 1 September 2005

Abstract

This present study revealed a dependence of rutile:anatase ratios in titania on the characteristics and catalytic properties of Co/TiO_2 catalysts during CO hydrogenation. In this study, Co/TiO_2 catalysts were prepared using various titania supports consisting of various rutile:anatase ratios of titania. In order to identify the characteristics, all catalyst materials were characterized using XRD, SEM/EDX, TPR, and hydrogen chemisorption. CO hydrogenation ($H_2/CO = 10/1$) was also performed to determine the overall activity and selectivity. It was found that both activity and selectivity were altered by changing the rutile:anatase ratios in the titania support.

Keywords: Cobalt catalyst; Titania; Chemisorption; CO; hydrogenation; Titania phase

1. Introduction

It has been known that supported cobalt (Co) catalysts are used for carbon monoxide (CO) hydrogenation because of their high activities based on natural gas [1], high selectivity to linear long chain hydrocarbons and also low activities for the competitive water–gas shift (WGS) reaction [2,3]. Many inorganic supports such as SiO_2 [4–8], Al_2O_3 [9–14], TiO_2 [15–17] and zeolites [18] have been extensively studied for supported Co catalysts for years. It is known that in general, the catalytic properties depend on reaction conditions, catalyst compositions, metal dispersion, and types of inorganic supports used. Thus, changes in the catalyst composition and/or even though the compositions of supports used may lead to significant enhanced catalytic properties as well.

During the past decades, titania-supported Co catalysts have been widely investigated by many authors, especially for the application of FT synthesis in a continuously stirred tank reactor (CSTR) [15–17]. However, it should be noted that titania itself has different crystalline phases such as anatase, brookite and rutile phase. Differences in crystalline phases may result in changes in physical and chemical properties of titania. Thus, different crystalline phase compositions of titania could play an important role on the catalytic performance of titania-supported Co catalysts during CO hydrogenation as well.

Therefore, the main objective of this present research was to investigate influences of various rutile:anatase ratios in titania support on the characteristics and catalytic properties during CO hydrogenation of Co/TiO_2 catalysts. In the present study, the Co/TiO_2 catalysts were prepared using various titania supports containing different ratios of rutile:anatase phase. The catalysts

* Corresponding author. Tel.: +662 218 6869; fax: +662 218 6766/6877.
E-mail address: bunjerd.j@chula.ac.th (B. Jongsomjit).

1566-7367/$ - see front matter © 2005 Elsevier B.V. All rights reserved.
doi:10.1016/j.catcom.2005.07.002

were characterized using various characterization techniques and tested in order to evaluate the catalytic properties during CO hydrogenation.

2. Experimental

2.1. Material preparation

2.1.1. Preparation of titania support

The various ratios of rutile:anatase in titania support were obtained by calcination of pure anatase titania (obtained from Ishihara Sangyo, Japan) in air at temperatures between 800 and 1000 °C for 4 h. The high space velocity of air flow (16,000 h^{-1}) insured the gradual phase transformation to avoid rapid sintering of samples. The ratios of rutile:anatase were determined by XRD according to the method described by Jung and Park [19] as follows:

$$\%\ \text{Rutile} = \frac{1}{[(A/R)0.884 + 1]} \times 100,$$

where A and R are the peak area for major anatase ($2\theta = 25°$) and rutile phase ($2\theta = 28°$), respectively.

2.1.2. Preparation of catalyst samples

A 20 wt% of Co/TiO_2 was prepared by the incipient wetness impregnation. A designed amount of cobalt nitrate [$Co(NO_3)\cdot 6H_2O$] was dissolved in deionized water and then impregnated onto TiO_2 containing various ratios of rutile:anatase obtained from Section 2.1.1. The catalyst precursor was dried at 110 °C for 12 h and calcined in air at 500 °C for 4 h.

2.2. Catalyst nomenclature

The nomenclature used for the catalyst samples in this study is following:

- *Rn:* titania support containing *n%* of rutile phase (R).
- *Co/Rn:* titania support containing *n%* of rutile phase (R)-supported cobalt.

2.3. Catalyst characterization

2.3.1. BET surface area

BET surface area of the samples with various rutile:anatase ratios of TiO_2 was performed to determine if the total surface area changes. It was determined using N_2 adsorption at 77 K in a Micromeritics ASAP 2010.

2.3.2. X-ray diffraction

XRD was performed to determine the bulk crystalline phases of catalyst. It was conducted using a SIEMENS D-5000 X-ray diffractometer with Cu $K\alpha(\lambda = 1.54439$ Å). The spectra were scanned at a rate of 2.4 deg/min in the range $2\theta = 20$–$80°$.

2.3.3. Scanning electron microscopy and energy dispersive X-ray spectroscopy

SEM and EDX were used to determine the catalyst morphologies and elemental distribution throughout the catalyst granules, respectively. SEM was carried out using a JEOL model JSM-5800LV. EDX was performed using Link Isis series 300 program.

2.3.4. Hydrogen chemisorption

Static H_2 chemisorption at 100 °C on the reduced cobalt catalysts was used to determine the number of reduced surface cobalt metal atoms. Prior to H_2 chemisorption, the catalyst sample was reduced in H_2 at 350 °C for 10 h. The resulting H_2 chemisorption is related to the overall activity of the catalysts during CO hydrogenation. Gas volumetric chemisorption at 100 °C was performed using the method described by Reuel and Bartholomew [20]. The experiment was performed in a Micromeritics ASAP 2010 using ASAP 2010C V3.00 software.

2.3.5. Temperature-programmed reduction

TPR was used to determine the reduction behaviors and reducibilities of the samples. It was carried out using 50 mg of a sample and a temperature ramp from 35 to 800 °C at 5 °C/min. The carrier gas was 5% H_2 in Ar. A cold trap was placed before the detector to remove water produced during the reaction. A thermal conductivity detector (TCD) was used to determine the amount of H_2 consumed during TPR. The H_2 consumption was calibrated using TPR of Ag_2O at the same conditions. The calculation of reducibilities was as described elsewhere [9,21–24].

2.4. Reaction

CO hydrogenation ($H_2/CO = 10/1$) was performed to determine the overall activity of the catalyst samples. Hydrogenation of CO was carried out at 220 °C and 1 atm. A flow rate of $H_2/CO/He = 20/2/8$ cm^3/min in a fixed-bed flow reactor under differential conditions was used. A relatively high H_2/CO ratio was used to minimize deactivation due to carbon deposition during reaction. Typically, 20 mg of a catalyst sample was reduced in situ in flowing H_2 (30 cm^3/min) at 350 °C for 10 h prior to the reaction. Reactor effluent samples were taken at 1 h intervals and analyzed by GC. In all cases, steady state was reached within 5 h.

3. Results and discussion

The present study showed the dependence of rutile: anatase ratios in titania on the catalytic properties during

CO hydrogenation of Co/TiO_2 catalysts. As mentioned, in general titania used contains mainly two phases; anatase and rutile phases. Phase transformation of titania depends on the preparation of titania such as sol–gel or solvothermal methods and also calcination temperatures. However, it was proposed that the different phase compositions in titania could play an important role on the catalytic properties during CO hydrogenation of Co/TiO_2 catalysts. Results and discussion are divided into two parts as follows.

3.1. Crystalline phases of titania

After calcination of the pure anatase titania under calcination temperatures ranging between 800 and 1000 °C for 4 h, the phase transformation from anatase to rutile phase should technically occur. The amounts of rutile phase formed during calcination depended on the temperature used. The high space velocity of the air flow at 16,000 h^{-1} was applied during the calcination process in order to minimize the rapid sintering due to the phase transformation of titania. It was found that after calcination of the pure anatase sample, the amounts of rutile phase obtained ranged between 3% and 99%. The titania supports containing rutile phase of ca. 0%, 3%, 19%, 40%, 96%, and 99% were named as R0, R3, R19, R40, R96, and R99, respectively. The surface areas of titania containing various rutile:anatase rations essentially decreased from 70 m^2/g for the R0 sample (pure anatase titania) to 49 m^2/g for the R99 sample (99% rutile titania). XRD patterns of titania samples calcined at various temperatures between 800 and 1000 °C are shown in Fig. 1. For the pure anatase titania (R0), XRD peaks of the anatase phase of titania at 25° (major), 37°, 48°, 55°, 56°, 62°, 71°, and 75° were evident. After calcination of the pure anatase titania sample, it was observed that besides the XRD peaks of pure anatase titania as shown above XRD peaks at 28° (major), 36°, 42°, and 57° were gradually seen. These peaks were assigned to the rutile phase essentially formed after calcination of the pure anatase titania. Apparently, the major peak at 28° of the rutile phase gradually increased with increasing the calcination temperatures indicating a higher content of rutile phase in the titania. It was shown that the transformation from anatase to rutile phase (R99) was almost complete at a temperature of ca. 1000 °C, resulting in the disappearance of XRD peaks for the anatase phase of titania. After various titania supports were obtained, the preparation of Co/TiO_2 with various rutile:anatase ratios of titania was consequently conducted in order to investigate the effect of the rutile:anatase ratio on characteristics and catalytic properties of the Co/TiO_2 catalysts during CO hydrogenation.

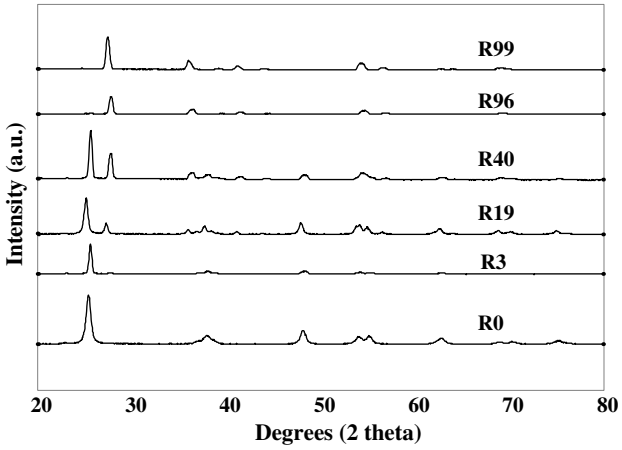

Fig. 1. XRD patterns for various ratios of rutile:anatase in titania supports.

3.2. Characteristics of Co/TiO_2

A 20 wt% of cobalt on titania supports containing various ratios of rutile:anatase phase was prepared by the conventional incipient wetness impregnation method. The XRD patterns for all calcined catalyst samples (Co/TiO_2) exhibited similar patterns as seen in Fig. 1. After calcination, all calcined samples exhibited XRD peaks, which were identical with those for the corresponding titania supports. This indicated that no further phase transformation from anatase to rutile occurred after calcination (at temperature ca. 500 °C for 4 h) of the catalyst samples. Besides the XRD peaks of the titania, all calcined samples also exhibited weak XRD peaks at 31°, 36°, and 65°, which were assigned to the presence of Co_3O_4. However, at high content of the rutile phase, the XRD peaks of Co_3O_4 were less apparent due to the strong intensity of XRD peaks for the rutile phase of titania. Based on the XRD results, it was clear that Co_3O_4 species were definitely present in a highly dispersed form.

SEM and EDX were also conducted in order to study the morphologies and elemental distribution of the catalyst samples, respectively. The typical SEM micrograph along with the EDX mapping (for Co, Ti, and O) are illustrated in Fig. 2 for the Co/R40 sample. The external surface of catalyst granule is shown in all figures and the light or white patches on the catalyst granule surface represent high concentration of cobalt oxides species on the surface. It can be seen that the cobalt oxide species were well dispersed and distributed (shown on mapping) all over the catalyst granule in all samples regardless of the ratio of rutile:anatase in the titania.

TPR was performed in order to identify the reduction behaviors and reducibility of catalysts. TPR profiles for all samples are shown in Fig. 3. TPR of the titania support samples used was also conducted at the same TPR conditions used for the catalyst samples (not shown) and no hydrogen consumption was detected.

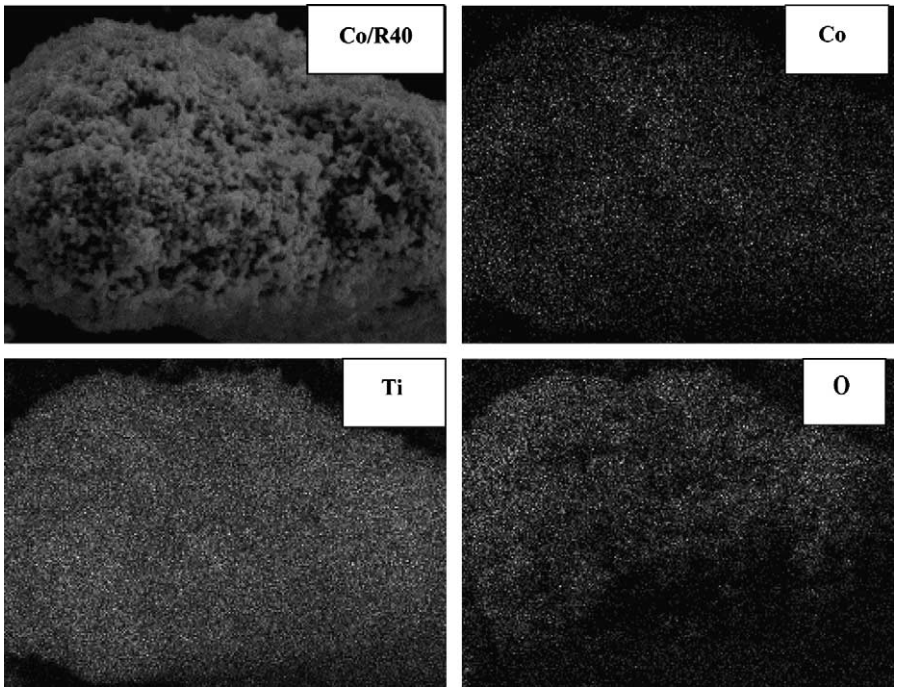

Fig. 2. A typical SEM micrograph for Co/R40 granule and EDX for Co, Ti, and O mapping.

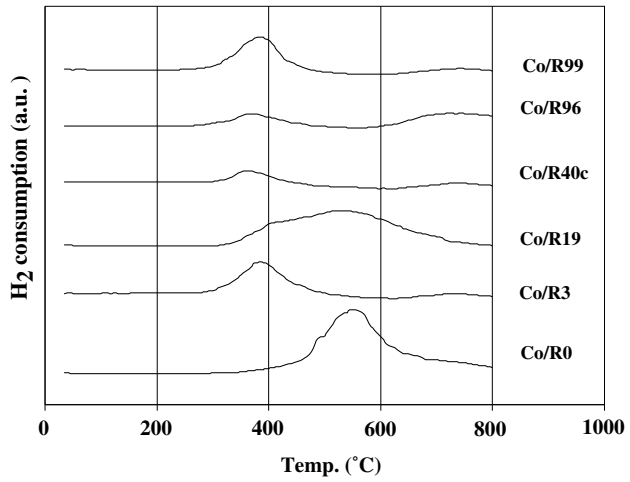

Fig. 3. TPR profiles for Co/TiO_2 catalysts with various ratios of rutile:anatase in titania supports used.

This indicated that the titania supports used themselves were not reducible at these TPR conditions. Apparently, TPR profiles of all calcined samples were similar exhibiting only one strong reduction peak as shown in Fig. 3. This peak can be assigned to the overlap of two-step reduction of Co_3O_4 to CoO and then to Co^0 [25]. Under TPR conditions, the two reduction peaks based on the two-step reduction may or may not be observed. The presence of only one reduction peak during TPR for all catalyst samples indicated that no residual cobalt nitrates precursor remained on the samples under the calcination condition used in this study. It was found that a TPR peak located at ca. 380–700 °C (max. at 520 °C) was observed for the Co/R0 sample. However, this reduction peak was dramatically shifted about 50–80 °C lower when ca. 3–99% of rutile phase (Co/R3 to Co/R99) was present in the titania supports used. This suggests that the presence of rutile phase in titania can facilitate the reduction process of cobalt oxide species on the titania support leading to reduction at a lower temperature. Since TPR is more of a bulk technique, it should be noted that the number of reduced Co metal obtained from the TPR measurement might not be well representative of the number of reduced Co metal surface atoms available for catalyzing CO hydrogenation. Therefore, static H_2 chemisorption on the reduced cobalt catalyst samples was used to determine the number of reduced Co metal surface atoms. This is usually related to the overall activity of the catalyst during CO hydrogenation.

The resulting H_2 chemisorption results for all catalyst samples are shown in Fig. 4. It was found that the amounts of H_2 adsorbed increased with the presence of rutile phase in titania up to a maximum at 19% of rutile phase (Co/R19) before decreasing when greater amounts of the rultile phase were present. Since H_2 chemisorption is a surface technique that the reduced Co metal surface atoms can be measured directly. The amounts of H_2 adsorbed on Co/TiO_2 obtained were lower compared to those for Co/Al_2O_3 and Co/SiO_2 at similar loading [5,6,21,22]. However, based on the H_2 chemisorption results in this present study, different ratios of rutile: anatase phase in titania exhibited different amounts of H_2 chemisorbed on the catalyst samples.

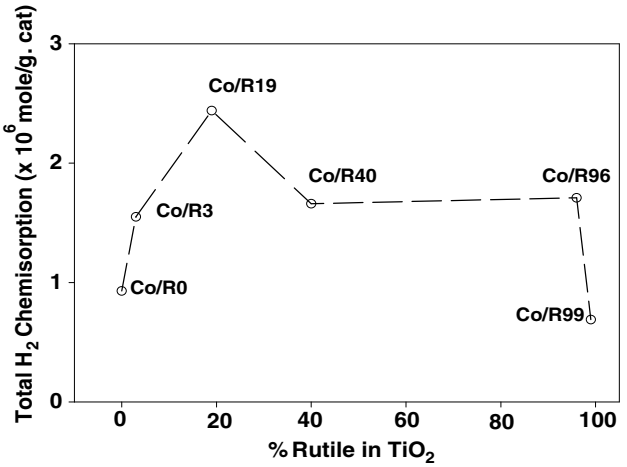

Fig. 4. H_2 chemisorption for Co/TiO_2 catalysts with various ratios of rutile:anatase in titania supports used.

3.3. Reactivity

In order to measure the catalytic properties of the catalyst samples with various ratios of rutile:anatase in titania, CO hydrogenation was performed in a fixed-bed flow reactor under differential condition. The results are shown in Fig. 5 and Table 1. It indicated that the reaction rate ranged between 0.3 and 6.6 μmole/g. cat. s (initial) and between 0.2 and 5.2 μmole/g cat s (steady state). This also showed that activities of the samples increased with the presence of rutile phase in titania up to a maximum at 19% of rutile phase (Co/R19) before decreasing when greater amounts of rutile phase were present, similar to the results obtained from H_2 chemisorption. Considering selectivity to methane, it was found that the presence of rutile phase in titania resulted in an increased selectivity to methane. After reaction, XRD of the spent catalyst samples was also

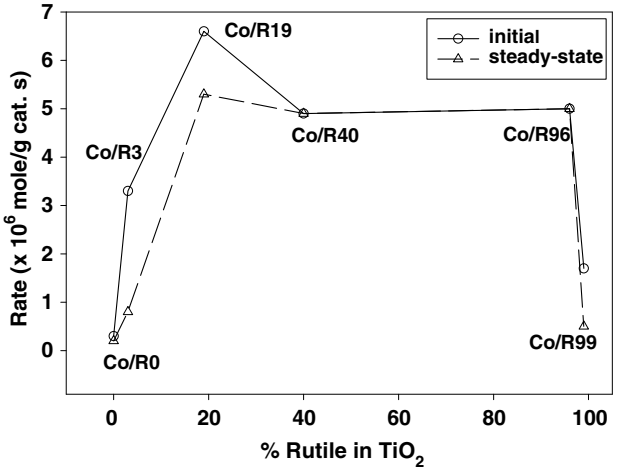

Fig. 5. Reaction rate during CO hydrogenation for Co/TiO_2 catalysts with various ratios of rutile:anatase in titania supports used.

Table 1
Activities and selectivity during CO hydrogenation of Co/TiO_2 via various rutile:anatase ratios of titania support

Catalyst samples	Rate (μmol/g cat s)[a]		Selectivity to CH_4(%)	
	Initial[b]	Steady state[c]	Initial[b]	Steady state[c]
Co/R0	0.3	0.2	71	68
Co/R3	3.3	0.8	99	99
Co/R19	6.6	5.3	98	98
Co/R40	4.9	4.9	97	96
Co/R96	5.0	5.0	99	99
Co/R99	1.7	0.5	94	94

[a] CO hydrogenation was carried out at 220 °C, 1 atm, and H_2/CO/He = 20/2/8.
[b] After 5 min of reaction.
[c] After 5 h of reaction.

performed in order to identify the bulk crystalline phases of the spent catalyst samples. It showed that the XRD patterns of all spent catalyst samples were identical with those of the corresponding fresh ones suggesting no phase changes occurred during the reaction condition used.

Based on the reaction study, it can be concluded that the catalytic properties of Co/TiO_2 depend on the ratio of rutile/anatase. The results revealed that the presence of rutile phase of an optimum of the rutile phase (i.e., Co/R19) result in an increased catalytic activity during CO hydrogenation. It is proposed that the presence of rutile phase in titania can facilitate the reduction process of cobalt oxides species resulting in lower reduction temperatures. The presence of some rutile phase also resulted in an increased number of reduced cobalt metal surface atoms available for catalyzing the reaction. However, higher ratios (more than 19%) of rutile:anatase in titania decreased the catalyst activities. It should be mentioned that besides the ratios of rutile:anatase in titania, there are also other factors such as preparation methods, titania precursors, particle sizes, modes and types of reactions that would affect the characteristics and catalytic properties of titania used both as a catalyst support or a catalyst itself.

4. Conclusion

The present research showed a dependence of the characteristics and catalytic properties during CO hydrogenation on the ratio of rutile/anatase in titania for Co. The study revealed that the presence of 19% rutile phase in titania for Co/TiO_2 (Co/R19) exhibited the highest activity during CO hydrogenation. It appeared that the increase in activity was due to two reasons;(i) the presence of rutile phase in titania can facilitrate the reduction process of cobalt oxide species into reduced cobalt metal and (ii) the presence of some rutile phase resulted in a larger number of reduced cobalt metal surface atoms, which is related to the activity during CO hydrogenation.

However, if the ratio of rutile:anatase was over 19%, the activity dramatically decreased. No further phase transformation of the supports occurred during calcination of the catalyst samples and reaction.

Acknowledgements

We gratefully acknowledge the financial support by the National Research Council of Thailand (NRCT), the Thailand Research Fund (TRF) and Thailand–Japan Technology Transfer Project (TJTTP-JBIC). We thank Prof. James G. Goodwin, Jr. at Clemson University for initiating this kind of project.

References

[1] A.P. Steynberg, M.E. Dry, B.H. Davis, B.B. Breman, in: Fischer-Tropsch Technology Study, Surface Science and Catalysis 152 (2004) 64.
[2] E. Iglesia, Appl. Catal. 161 (1997) 59.
[3] R.C. Brady, R.J. Pettie, J. Am. Chem. Soc. 103 (1981) 1287.
[4] A. Martinez, C. Lopez, F. Marquez, I. Duaz, J. Catal. 220 (2003) 486.
[5] J. Panpranot, J.G. Goodwin Jr., A. Sayari, Catal. Today 77 (2002) 269.
[6] J. Panpranot, J.G. Goodwin Jr., A. Sayari, J. Catal. 211 (2002) 530.
[7] S.L. Sun, I. Isubaki, K. Fujimoto, Appl. Catal. 202 (2000) 121.
[8] S. Ali, B. Chen, J.G. Goodwin Jr., J. Catal. 157 (1995) 35.
[9] B. Jongsomjit, J. Panpranot, J.G. Goodwin Jr., J. Catal. 215 (2003) 66.
[10] T. Das, G. Jacobs, P.M. Patterson, W.A. Conner, J.L. Li, B.H. Davis, Fuel 82 (2003) 805.
[11] G. Jacobs, P.M. Patterson, Y.Q. Zhang, T. Das, J.L. Li, B.H. Davis, Appl. Catal. 233 (2002) 215.
[12] M. Rothaemel, K.F. Hanssen, E.A. Blekkan, D. Schanke, A. Holmen, Catal. Today 38 (1997) 79.
[13] V. Ragaini, R. Carli, C.L. Bianchi, D. Lorenzetti, G. Vergani, Appl. Catal. 139 (1996) 17.
[14] V. Ragaini, R. Carli, C.L. Bianchi, D. Lorenzetti, G. Predieri, P. Moggi, Appl. Catal. 139 (1996) 31.
[15] J.L. Li, G. Jacobs, T. Das, B.H. Davis, Appl. Catal. 233 (2002) 255.
[16] G. Jacobs, T. Das, Y.Q. Zhang, J.L. Li, G. Racoillet, B.H. Davis., Appl. Catal. 233 (2002) 263.
[17] J.L. Li, L.G. Xu, R. Keogh, B.H. Davis, Catal. Lett. 70 (2000) 127.
[18] X.H. Li, K. Asami, M.F. Luo, K. Michiki, N. Tsubaki, K. Fujimoto, Catal. Today 84 (2003) 59.
[19] K.Y. Jung, S.B. Park, J. Photochem. Photobiol. A. 127 (1999) 117.
[20] R.C. Reuel, C.H. Bartholomew, J. Catal. 85 (1984) 63.
[21] B. Jongsomjit, J. Panpranot, J.G. Goodwin Jr., J. Catal. 204 (2001) 98.
[22] B. Jongsomjit, J.G. Goodwin Jr., Catal. Today 77 (2002) 191.
[23] A. Kogelbauer, J.C. Weber, J.G. Goodwin Jr., Catal. Lett. 34 (1995) 269.
[24] Y. Zhang, D. Wei, S. Hammache, J.G. Goodwin Jr., J. Catal. 188 (1999) 281.
[25] B. Jongsomjit, C. Sakdamnuson, J.G. Goodwin Jr., P. Praserthdam, Catal. Lett. 94 (2004) 209.

Available online at www.sciencedirect.com
SCIENCE DIRECT
Catalysis Communications 7 (2006) 192–197
CATALYSIS COMMUNICATIONS
www.elsevier.com/locate/catcom

Differences in characteristics and catalytic properties of Co catalysts supported on micron- and nano-sized zirconia

Joongjai Panpranot *, Nuttakarn Taochaiyaphum, Bunjerd Jongsomjit, Piyasan Praserthdam

Center of Excellence on Catalysis and Catalytic Reaction Engineering, Department of Chemical Engineering, Faculty of Engineering, Chulalongkorn University, Phayathai Road, Bangkok 10330, Thailand

Received 15 August 2005; received in revised form 17 October 2005; accepted 21 October 2005
Available online 27 December 2005

Abstract

Nanocrystalline zirconia was prepared by decomposition of zirconium tetra *n*-propoxide in 1,4-butanediol and was employed as a support for cobalt catalysts. The activity and the selectivity of the catalysts in CO hydrogenation were compared with cobalt supported on commercial available micron- and nano-sized zirconia. The catalytic activities were found to be in the order: Co/ZrO_2-nano-glycol $\gg$ Co/ZrO_2-nano-com > Co/ZrO_2-micron-com. Compared to the micron-sized zirconia supported one, the use of commercial nano-sized zirconia resulted in higher CO hydrogenation activity but lower selectivity for longer chain hydrocarbons (C_4–C_6), whereas the use of glycothermal-derived nanocrystalline zirconia exhibited both higher activity and selectivity for C_4–C_6. The better performance of the latter catalyst can be ascribed to not only the effect of the crystallite size but also the presence of pure tetragonal phase of zirconia.

Keywords: Nanocrystalline zirconia; CO hydrogenation; Cobalt catalyst; Glycothermal method

1. Introduction

Zirconia powder has been effectively used in different areas of chemistry such as in ceramics and catalysis. It has been found that zirconia has high catalytic activities for isomerization of olefins [1] and epoxides [2]. Use of zirconia as a catalyst support has shown promising results in many environmental catalysis reactions such as CO_2 hydrogenation [3], CO oxidation [4], and Fischer–Tropsch reaction [5–7]. Enache et al. reported that compared to conventional alumina supported Co catalysts, the ones supported on zirconia showed better reducibility and capable of hydrogen adsorption via spillover mechanism. The authors proposed that these properties resulted in a higher catalytic activity and an increase of the chain growth probability in the Fischer–Tropsch reaction. Recently, we reported the synthesis and characteristics of nanocrystalline zirconia prepared by glycothermal method using various glycols and their applications as cobalt catalyst supports [8]. Cobalt-based catalysts are known to be commercially attractive for natural gas-based Fischer–Tropsch synthesis because of their high activities, high selectivities for long chain paraffins, low water–gas shift activities, and their relatively low price compared to noble metals such as Ru [9–11].

In this work, the characteristics and catalytic properties of nanocrystalline zirconia supported Co catalysts were studied and compared to commercially available micron- and nano-sized zirconia supported ones. The physicochemical properties of the catalysts were analyzed by means of thermal gravimetric analysis (TGA), X-ray diffraction (XRD), N_2 physisorption, scanning electron microscopy (SEM), and H_2 chemisorption. The catalytic performances of the zirconia supported Co catalysts were tested in CO hydrogenation reaction at 220 °C and 1 atm.

* Corresponding author. Tel.: +66 2 218 6859/78; fax: +66 2 218 6877.
E-mail address: joongjai.p@eng.chula.ac.th (J. Panpranot).

1566-7367/$ - see front matter © 2005 Elsevier B.V. All rights reserved.
doi:10.1016/j.catcom.2005.10.007

2. Experimental

2.1. Catalyst preparation

Nanocrystalline zirconia with the average crystallite size of 4 nm was prepared by the glycothermal method according to the procedure described in [12]. Approximately 15 g of zirconium tetra *n*-propoxide, $Zr(OC_3H_7)_4$ (ZNP) with 20.5% Zr from Strem Chemicals was added to 100 ml of 1,4-butanediol (Aldrich). This mixture was placed in a 300-ml autoclave. After the atmosphere inside the autoclave was replaced with nitrogen, the mixture was heated to 300 °C at a heating rate of 2.5 °C/min and was kept at that temperature for 2 h. After cooling to room temperature, the resulting powders were collected and washed repeatedly with methanol by vigorous mixing and centrifuging. Concentrated ammonium hydroxide was added to the upper part of the mixture, if no additional particle settling was observed then washing was finished. The products were then air-dried and were used without further calcination. Commercial zirconias in micron- and nano-sized were obtained from Aldrich for comparison purposes. The zirconia supported Co catalysts were prepared by the incipient wetness impregnation of the supports with aqueous solution of Co(II) nitrate hexahydrate (Aldrich). The samples were dried at 110 °C for 1 day and then were calcined in air at 300 °C for 2 h. The final cobalt loading of the calcined catalysts were determined using atomic absorption spectroscopy (Varian Spectra A800) to be ca. 8 wt%.

2.2. Catalyst characterization

TGA was performed using a DIAMOND TG/DTA analyzer. The catalyst samples of 10–20 mg and a temperature ramping from 35 to 800 °C at 10 °C/min were used in the operation. The carrier gas was N_2 UHP. The BET surface areas were determined by N_2 physisorption using a Quantachrome Nova 1000 automated system. Each sample was degassed in the system at 150 °C for 2 h prior to N_2 physisorption. The XRD spectra of the sample powders were measured using a SIEMENS D5000 X-ray diffractometer using Cu K_α radiation with a Ni filter in the 10–80° 2θ angular regions. The particle morphology was obtained using a JEOL JSM-35CF scanning electron microscope (SEM) operated at 20 kV. Transmission electron microscopy was performed on a JEOL-TEM 200CX transmission electron microscope operated at 100 kV. The catalyst sample was first suspended in ethanol using ultrasonic agitation for 10 min. The suspension was dropped onto a thin Formvar film supported on copper grid and dried at room temperature before observation. H_2 chemisorption was carried out following the procedure described by Reuel and Bartholomew [13] using a Micromeritics Pulse Chemisorb 2700 system. Prior to chemisorption, the catalysts were reduced at 350 °C for 10 h after ramping at a rate of 1 °C/min. Static H_2 chemisorption was performed at 100 °C.

2.3. CO hydrogenation reaction

CO hydrogenation was carried out at 220 °C and 1 atm total pressure in a fixed-bed stainless steel reactor under differential conversion conditions. A flow rate of $H_2/CO/Ar = 20/2/8$ cm^3/min was used. Typically, 0.2 g of the catalyst samples were reduced in situ in flowing H_2 (50 cm^3/min) at 350 °C for 10 h prior to reaction. The data was collected every hour and analyzed by gas chromatography. The steady-state rates for all the catalysts were obtained after 5–6 h. The percentages of CO conversion and reaction rates were defined as:

$$\%\text{CO conversion} = \frac{(\text{mol of CO in feed} - \text{mol of CO in products})}{(\text{mol of CO in feed})} \times 100,$$

$$\text{Reaction rate}\,(\text{g CH}_2\,\text{g cat.}^{-1}\,\text{h}^{-1}) = \frac{\%\text{CO conversion} \times \text{flowrate of CO in feed}\,(\text{cm}^3/\text{min}) \times 60\,(\text{min}/\text{h}) \times \text{mol. wt of CH}_2\,(\text{g/mol})}{\text{catalyst weight}\,(\text{g}) \times 22{,}400\,(\text{cm}^3/\text{mol})}.$$

3. Results and discussion

Fig. 1 shows the scanning electron micrographs of micron- and nano-sized zirconia before and after cobalt loading. It was found that the commercial micron-sized zirconia have a spherical shape with an average particle size of ca. 0.2 μm. The SEM micrographs of the commercial nano-sized zirconia showed very small particle sizes that appeared to be more agglomerated. Compared to the commercial available ones, the glycothermal-derived nanocrystalline zirconia appeared as large separate spherical particles (1 μm). These particles were formed by aggregation of their primary particles. The mechanism during crystallization of zirconia in the glycols during glycothermal synthesis has been suggested in our previous study [12]. Nanocrystals were formed when starting materials were completely dissolved into the glycol. Crystallization of the glycoxide intermediates in 1,4-butanediol then proceeds via solid-state transformation. After impregnated with solutions of cobalt nitrate, dried overnight at room temperature, and calcination at 300 °C for 2 h, the morphologies of the commercial micron- and nano-sized zirconia supported catalysts were found to be more agglomerated especially the nano-sized ones. High concentration of

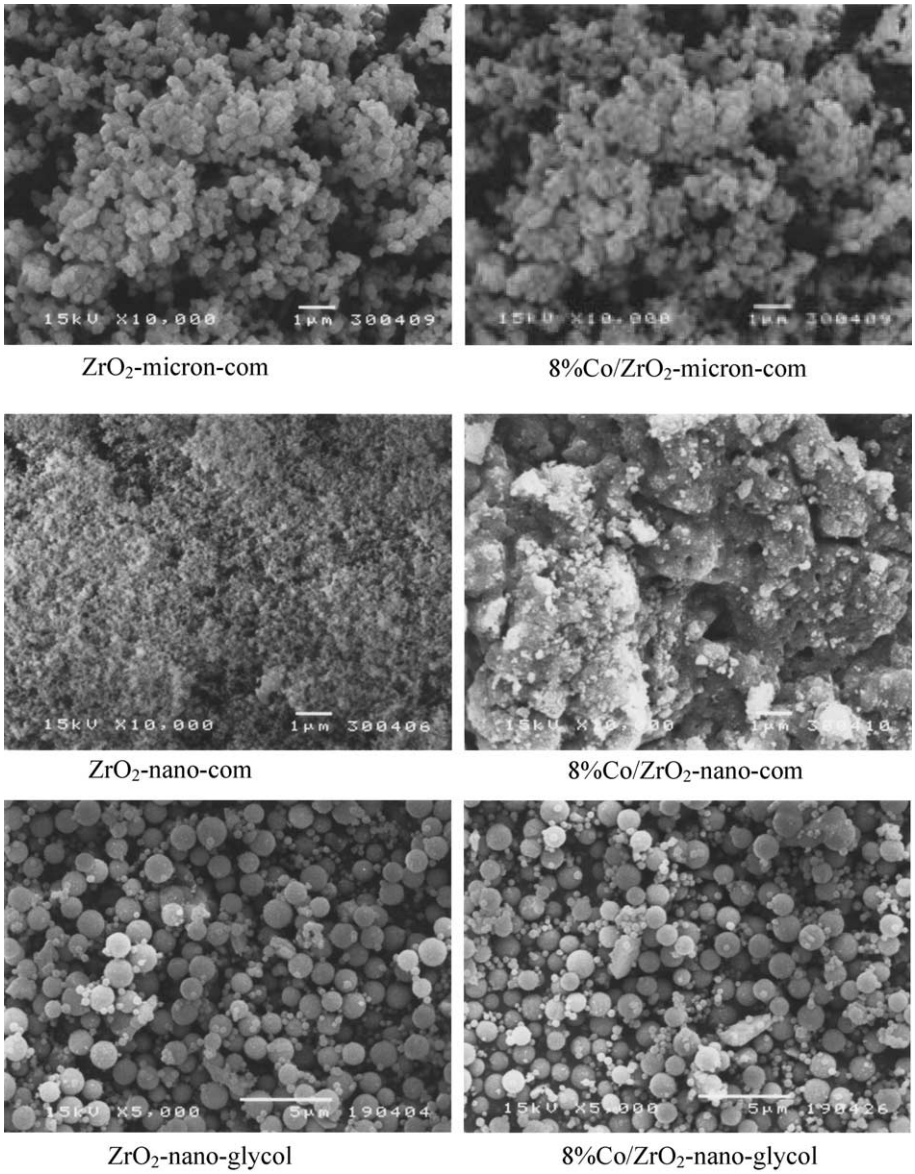

Fig. 1. SEM micrographs of various ZrO_2 and 8%Co/ZrO_2 catalysts.

cobalt appeared as light/white spots on the granules of the Co/ZrO_2-nano-com catalyst. Unlike the commercial zirconia supported Co catalysts, the morphology of the glycothermal-derived nanocrystalline zirconia supported one was not altered by cobalt impregnation and calcination even for cobalt loading as high as 8 wt%.

The X-ray diffraction patterns of the various ZrO_2 are shown in Fig. 2. Both micron- and nano-sized commercial zirconia samples exhibited the XRD patterns of both tetragonal and monoclinic zirconia while only tetragonal phase was obtained for the glycothermal-derived ones. Typically, the monoclinic phase is stable to ≈1170 °C, at which temperature it transforms into the tetragonal phase, which is stable up to 2370 °C [14]. However, at low temperature, a metastable tetragonal phase zirconia is usually observed when zirconia is prepared by certain methods such as precipitation from aqueous salt solution or thermal composition of zirconium salts as employed in this work. It is also found that there was less monoclinic phase for the commercial nano-sized zirconia compared to the micron-sized one. The transformation of the metastable tetragonal form into the monoclinic form was due probably to the lower surface energy of the tetragonal phase compared to monoclinic phase [15,16]. The average crystallite sizes of tetragonal and monoclinic zirconia determined by X-ray line broadening and BET surface areas of the zirconia samples are given in Table 1. The average crystallite size of tetragonal phase of the glycothermal-derived zirconia was calculated to be 4 nm while those of commercial ones were ca. 9–12 nm. The BET surface areas of the catalyst samples were 50–170 m^2/g in the order of Co/ZrO_2-nano-glycol ≫ Co/ZrO_2-nano-com > Co/ZrO_2-micron-com. The information on porosity of the new nanocrystalline ZrO_2 such as pore volumes and N_2 adsorption–desorption iso-

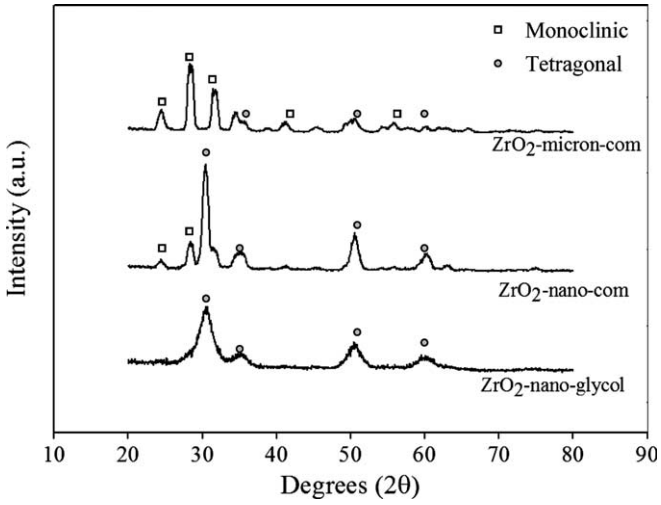

Fig. 2. XRD patterns of various ZrO_2 samples.

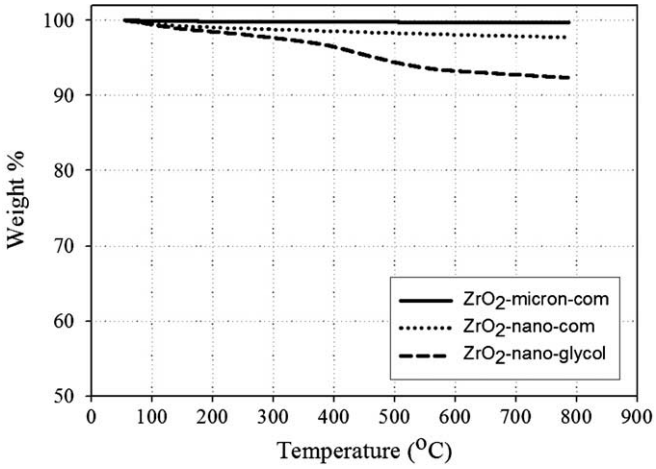

Fig. 3. TGA profiles of various ZrO_2 samples.

therms can be found in [12]. After impregnation of cobalt and calcination at 300 °C, the XRD peaks for cobalt oxides were not apparent for all the catalyst samples due probably to overlapping of Co_3O_4 peaks with those of the ZrO_2 supports. Thermal stability of the zirconia samples was investigated by thermal gravimetric analysis and the results are shown in Fig. 3. It was found that the ZrO_2-nano-glycol exhibited ≈8% and 5% more weight loss than those of ZrO_2-micron-com and ZrO_2-nano-com, respectively, during heat treatment up to 800 °C. These losses may be due to larger amount of water was adsorbed on the high surface area/pore volume ZrO_2-nano-glycol and not to the phase change as confirmed by XRD (results not shown).

The H_2 chemisorption results and the catalytic activities of zirconia supported Co catalysts are reported in Tables 1 and 2, respectively. We have performed CO hydrogenation under methanation conditions (high H_2/CO ratio) in order to minimize deactivation of the catalysts due to wax formation. It is clearly seen that the catalysts supported on nano-sized zirconia exhibited smaller Co° particle size, higher Co dispersion, and higher CO hydrogenation activities than the micron-sized supported one with the use of the glycothermal-derived nanocrystalline zirconia showed the best performances. As reported in the literature, strong metal support interaction (SMSI) between metal (i.e. Pt) and ZrO_2 occurs during high temperature reduction ⩾850 °C [17]. Under the reduction and reaction temperatures used in this study (350 and 220 °C, respectively), the SMSI effect is likely to be absent. Thus, a decrease in cobalt oxide particle size (as surface area of ZrO_2 increases) can result in faster reduction due to a greater surface area/volume ratio hence higher metal dispersion can be obtained.

It should be noted that under similar reaction conditions (methanation) relatively large portions of higher hydrocarbons (C_4–C_6) were obtained on all the Co/ZrO_2 catalysts compared to those reported in the literature for Co catalysts supported on SiO_2 [18], Al_2O_3 [19], or TiO_2 [20]. It is likely that the use of ZrO_2 support significantly enhances the polymerization reaction as also suggested by Enache et al. [7]. In this study, we report that compared to the use of micron-size ZrO_2, the nano-sized ones exhibited even higher selectivities for long chain hydrocarbons. However, for the two commercial zirconia supported Co catalysts, the product selectivities were similar in which $C_1 \gg C_4$–$C_6 > C_2$–C_3, typical for CO hydrogenation under methanation while for the glycothermal-derived nanocrystalline ZrO_2 supported catalyst, the selectivities for longer chain hydrocarbons were much higher and were found to be in the order: C_4–$C_6 \gg C_1 > C_2$–C_3. In other words, using

Table 1
The characteristics of Co/ZrO_2 catalysts

Sample	BET S.A.[a] (m^2/g)	Crystal size of ZrO_2[b] (nm)		H_2 chemisorption[d] ($\times 10^{19}$ mol g cat.$^{-1}$)	% Co dispersion[e]	d_P Co[0f] (nm)
		Tetragonal	Monoclinic			
Co/ZrO_2-micron-com	50	7.7	10.5	3.1	7.6	12.6
Co/ZrO_2-nano-com	78	11.5	10.2	10.1	24.7	3.9
Co/ZrO_2-nano-glycol	170	4.0	n.d.[c]	15.3	37.4	2.6

[a] Error of measurements = ±10%.
[b] Determined by XRD line broadening using Scherrer's equation [21].
[c] n.d. = not detected.
[d] Error of measurement = ±5%.
[e] Based on total amount of cobalt.
[f] $d_P = 5/(S_{Co} \times \rho_{Co})$, where S_{Co} is the surface area of cobalt measured by H_2 chemisorption.

Table 2
Catalytic activities of Co/ZrO_2 in CO hydrogenation

Catalysts	Reaction rate[a] ($g\ CH_2\ g\ cat^{-1}\ h^{-1}$)	Product selectivity (%)			TOFs[b] (s^{-1})
		C_1	C_2–C_3	C_4–C_6	
Co/ZrO_2-micron-com	1.7	57.8	14.4	17.8	0.66
Co/ZrO_2-nano-com	3.8	77.8	8.6	13.5	0.45
Co/ZrO_2-nano-glycol	14.5	29.5	11.4	59.1	1.13

[a] Reaction conditions were 220 °C, 1 atm and H_2/CO ratio = 10.
[b] Based on H_2 chemisorption results.

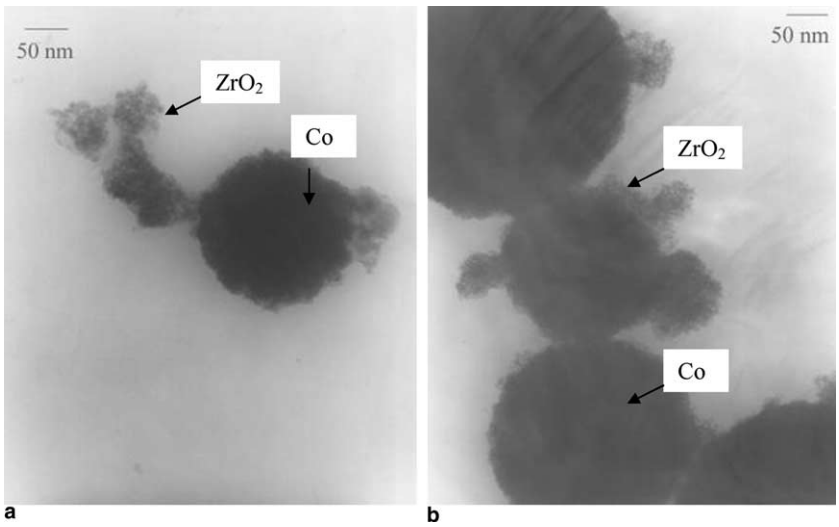

Fig. 4. TEM micrographs of Co/ZrO_2-nano-glycol: (a) before and (b) after CO hydrogenation reaction at 220 °C 1 atm for 6 h.

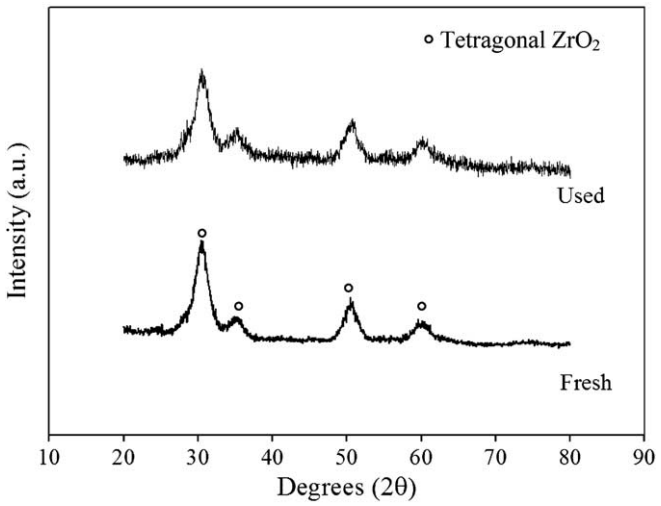

Fig. 5. XRD patterns of Co/ZrO_2-nano-glycol before and after used in CO hydrogenation reaction at 220 °C and 1 atm for 6 h.

the nano-sized zirconia resulted in higher CO hydrogenation rates but on the expense of selectivities for C_4–C_6, whereas Co catalyst supported glycothermal-derived nanocrystalline zirconia, both higher reaction rate and higher selectivities for longer chain hydrocarbons were obtained. Thus, it is not only the effect of ZrO_2 crystallite size but also the presence of pure tetragonal phase of zirconia that resulted in better catalytic performances in CO hydrogenation. Stabilization of tetragonal phase zirconia has been reported to be very important for applications as a catalyst or catalyst support [5]. The TEM micrographs and the XRD patterns of Co/ZrO_2-nano-glycol catalyst before and after CO hydrogenation reaction are shown in Figs. 4 and 5, respectively. Primary particles in nano-sized of the glycothermal-derived ZrO_2 as well as high Co dispersion can be observed for both fresh and used catalysts. There was also no change in the tetragonal phase of the ZrO_2 while the crystallite size was slightly increased from 4.0 to 4.3 nm. Overall, the results in this study suggest a marginal effect of the nanocrystalline zirconia on the catalytic activities and selectivities on CO hydrogenation reaction. Although the cost of catalyst preparation using glycothermal process is more expensive than conventional method, their unique properties such as high stability of pure tetragonal ZrO_2 offer interesting possibilities for catalyst design and for application in particular cases.

4. Conclusions

The comparison of catalytic performances in CO hydrogenation of the cobalt catalysts supported on glycothermal-derived nanocrystalline zirconia and commercial available nano- and micron-sized zirconia shows that both catalyst

activity and selectivity for long chain hydrocarbons were enhanced by the use of nanocrystalline zirconia as catalyst supports. The glycothermal-derived catalysts exhibited higher surface areas, higher Co dispersion, and highly stable pure tetragonal phase zirconia.

References

[1] Y. Nakano, T. Iizuka, H. Hattori, K. Tanabe, H. Hideshi, T. Kozo, J. Catal. 157 (1979) 1.
[2] K. Arata, K. Kato, K. Tanabe, Bull. Chem. Soc. Jpn. 49 (1976) 563.
[3] J.H. Bitter, K. Sechan, J.A. Lercher, J. Catal. 171 (1997) 279.
[4] W.P. Dow, T.J. Huang, J. Catal. 147 (1994) 322.
[5] G.K. Chuah, Catal. Today 49 (1999) 131.
[6] L. Bruce, J.F. Mathews, Appl. Catal. 4 (1982) 353.
[7] D.I. Enache, M. Roy-Auberger, R. Revel, Appl. Catal. A: General 268 (2004) 51.
[8] J. Panpranot, N. Taochaiyaphum, P. Praserthdam, Mater. Chem. Phys. 94 (2005) 207.
[9] R.B. Anderson, The Fischer–Tropsch Synthesis, Academic Press, San Diego, 1984.
[10] J.G. Goodwin Jr., Prep. ACS Div. Petr. Chem. 36 (1991) 156.
[11] E. Iglesia, Appl. Catal. A 161 (1997) 50.
[12] S. Kongwudthiti, P. Praserthdam, P.L. Silveston, M. Inoue, Ceram. Int. 29 (2003) 807.
[13] R.C. Reuel, C.H. Bartholomew, J. Catal. 85 (1984) 78.
[14] P.D.L. Mercera, J.G. van Ommen, E.B.M. Doesburg, A.J. Burggraaf, J.R.H. Ross, Appl. Catal. 71 (1991) 363.
[15] E. Tani, M. Yoshimura, S. Somiya, J. Am. Ceram. Soc. 66 (1982) 11.
[16] M.I. Osendi et al., J. Am. Ceram. Soc. 68 (1985) 135.
[17] J.H. Bitter, K. Seshan, J.A. Lercher, J. Catal. 171 (1997) 279–286.
[18] J. Panpranot, S. Kaewgun, P. Praserthdam, React. Kinet. Catal. Lett. 85 (2005) 299.
[19] B. Jongsomjit, J.G. Goodwin Jr., Catal. Today 77 (2002) 191.
[20] B. Jongsomjit, T. Wongsalee, P. Praserthdam, Catal. Commun. 6 (2005) 705.
[21] H.P. Klug, L.E. Alexander, X-ray Diffraction Procedures for Polycrystalline Amorphous Materials, second ed., Wiley, New York, 1974.

ELSEVIER

Science and Technology of Advanced Materials 6 (2005) 290–295

SCIENCE AND TECHNOLOGY OF ADVANCED MATERIALS

www.elsevier.com/locate/stam

Activity of nanosized titania synthesized from thermal decomposition of titanium (IV) *n*-butoxide for the photocatalytic degradation of diuron

Jitlada Klongdee[a], Wansiri Petchkroh[b], Kosin Phuempoonsathaporn[c], Piyasan Praserthdam[a], Alisa S. Vangnai[b,d], Varong Pavarajarn[a,*]

[a]*Department of Chemical Engineering, Faculty of Engineering, Center of Excellence on Catalysis and Catalytic Reaction Engineering, Chulalongkorn University, Bangkok 10330, Thailand*

[b]*National Research Center for Environmental and Hazardous Waste Management (NRC-EHWM), Chulalongkorn University, Bangkok 10330, Thailand*

[c]*Biotechnology Graduate Program, Faculty of Science, Chulalongkorn University, Bangkok 10330, Thailand*

[d]*Department of Biochemistry, Faculty of Science, Chulalongkorn University, Bangkok 10330, Thailand*

Received 12 January 2005; revised 15 February 2005; accepted 15 February 2005
Available online 17 June 2005

Abstract

Nanoparticles of anatase titania were synthesized by the thermal decomposition of titanium (IV) *n*-butoxide in 1,4-butanediol. The powder obtained was characterized by various characterization techniques, such as XRD, BET, SEM and TEM, to confirm that it was a collection of single crystal anatase with particle size smaller than 15 nm. The synthesized titania was employed as catalyst for the photodegradation of diuron, a herbicide belonging to the phenylurea family, which has been considered as a biologically active pollutant in soil and water. Although diuron is chemically stable, degradation of diuron by photocatalyzed oxidation was found possible. The conversions achieved by titania prepared were in the range of 70–80% within 6 h of reaction, using standard UV lamps, while over 99% conversion was achieved under solar irradiation. The photocatalytic activity was compared with that of the Japanese Reference Catalyst (JRC-TIO-1) titania from the Catalysis Society of Japan. The synthesized titania exhibited higher rate and efficiency in diuron degradation than reference catalyst. The results from the investigations by controlling various reaction parameters, such as oxygen dissolved in the solution, diuron concentration, as well as light source, suggested that the enhanced photocatalytic activity was the result from higher crystallinity of the synthesized titania.

Keywords: Titania; Thermal decomposition; Nanoparticle; Photocatalytic activity; Diuron; Degradation

1. Introduction

Titanium (IV) dioxide or titania (TiO_2) is one of the most common metal-oxides recognized in various industries. Due to its good physical and chemical properties, such as catalytic activity [1], photocatalytic activity [2], good stability toward adverse environment [3], sensitivity to humidity and gas [4], dielectric character [5], nonlinear optical characteristic [6] and photoluminescence [7], titania has been used in many fields of application including the use as catalysts, catalyst supports, electronics, cosmetics, pigments and filler coating. Nevertheless, photocatalyst is one of the most important applications of titania. Although titania is known to have three natural polymorphs, i.e. rutile, anatase, and brookite, only anatase is generally accepted to have significant photocatalytic activity [8–10].

Many factors affect the photocatalytic activity of titania. Particle size is one of the most important factors. It has been reported that photocatalytic activity is increased with the decrease in titania particle size, especially into nanometer-scale, because of high surface area and short interface migration distances for photoinduced holes and electrons [11–13]. Nanocrystalline titania can be synthesized by many methods, such as sol-gel method, hydrothermal method, vapor-phase hydrolysis, laser-induced decomposition, chemical vapor decomposition and molten salt method. In this work, nanocrystalline anatase titania was synthesized via the thermal decomposition of titanium alkoxide in organic solvent, which has been employed to synthesize various nanocrystalline metal-oxides [14–19]. It has been

* Corresponding author. Tel.: +66 2 2186 890; fax: +66 2 2186 877.
E-mail address: fchvpv@eng.chula.ac.th (V. Pavarajarn).

1468-6996/$ - see front matter © 2005 Elsevier Ltd. All rights reserved.
doi:10.1016/j.stam.2005.02.007

demonstrated that the activity of titania synthesized by this method is much higher than those of commercially available titania for photocatalytic decomposition of simple compound, such as acetic acid, in aqueous solutions [20]. However, it has never been used for the decomposition of more complex substance. In this study, photodegradation of complex substance, i.e. diuron [3-(3,4-dichlorophynyl)-1,1-dimethylurea], is employed to investigate the activity of titania prepared by this method.

Diuron has been one of the most commonly used herbicides for more than 40 years. It is bio-recalcitrant and chemically stable with half-life in soil over 300 days. Since, diuron is slightly soluble (solubility of 36.4 mg/l at 25 °C), it can slowly penetrates through soil and contaminates underground water. Photodegradation using titania as catalyst is therefore one potential option for contaminated water remediation.

2. Materials and methods

2.1. Synthesis of titania

Titanium (IV) *n*-butoxide (TNB) was used as starting material for titania synthesis. 15 g of TNB was suspended in 100 ml of 1,4-butanediol, which was used as reaction medium, in a test tube. The test tube was then placed in a 300 ml autoclave. The gap between the test tube and the autoclave wall was also filled with 1,4-butanediol. The autoclave was purged completely by nitrogen before heating up to 300 °C at a rate of 2.5 °C/min. Autogeneous pressure during the reaction gradually increased as the temperature was raised. The system was held at 300 °C for 2 h before cooling down to room temperature. The resulting powders in the test tube were repeatedly washed with methanol and dried in 110 °C oven overnight. Subsequently, the obtained product was calcined at 500 °C for 2 h in a box furnace with a heating rate of 10 °C/min.

Synthesized powders were characterized by various techniques, i.e. powder X-ray diffraction (XRD), scanning electron microscope (SEM) and transmission electron microscope (TEM). Powder X-ray diffraction (XRD) analysis was done by using a SIEMENS D5000 diffractometer with CuKα radiation. The crystallite size of the product was determined from the broadening of its main peak, using the Scherrer equation. Specific surface area of the samples was also measured by using the BET multipoint method.

2.2. Photocatalytic experiments

Photodegradation of diuron in aqueous solution was employed to investigate the photocatalytic activity of the synthesized titania. The initial concentrations of diuron used were 1 and 10 ppm, respectively. The solution was mixed with titania in the ratio of 1 mg titania to 10 ml of solution and kept in the dark for at least 15 min to allow the complete adsorption of diuron on the surface of titania. The photocatalytic reaction was initiated by exposing test tubes to light from UV lamps (Phillips Cleo 15 W). Diuron degradation was periodically monitored by using a reverse phase HPLC system. The HPLC system included Hyperclone column (150×8 mm inner diameter; 5 μm particle size) (Phenomenex, USA) with a mobile phase of 70% acetonitrile–29.5% water–0.5% phosphoric acid; a flow rate of 0.5 ml/min and a UV detector at 254 nm. The photocatalytic activity of the synthesized catalyst was compared with that of the Japanese Reference Catalyst titania, JRC-TIO-1, which is also pure nanocrystalline anatase.

3. Results and discussion

3.1. Properties of synthesized titania

The particles obtained from the decomposition of TNB in 1,4-butanediol at 300 °C was confirmed to be titania. The XRD analysis, as shown in Fig. 1, revealed that the synthesized product before calcination was already anatase phase. This result was in agreement with the results from our previous work that anatase crystals were formed by crystallization when the temperature in the autoclave reached 250 °C [21]. The crystallite size of the as-synthesized product calculated from the Scherrer equation was approximately 13 nm, while that of the calcined product was 15 nm. It should be noted that the crystallite sizes calculated were in agreement with TEM observation (Fig. 2). Therefore, it was suggested that the synthesized product synthesized was nanosized single crystal titania.

As shown in Table 1, the BET surface area measured by nitrogen adsorption (S_{BET}) of the as-synthesized products was comparable with the surface area calculated from the particle size (S_{XRD}), which was assumed that the particles were spherical and nonporous. It was therefore suggested

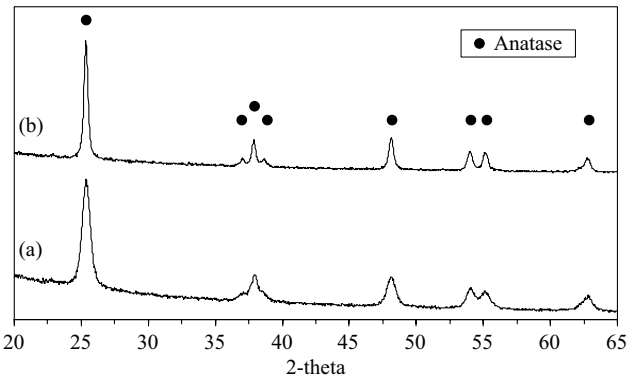

Fig. 1. XRD patterns of synthesized titania: (a) before calcination, (b) after calcination.

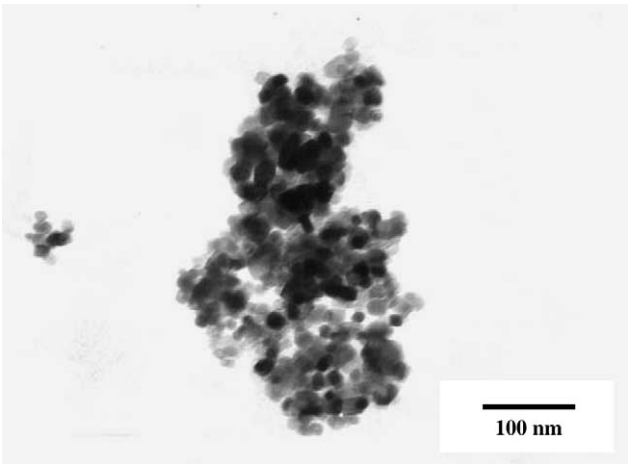

Fig. 2. TEM micrograph of as-synthesized titania.

that the primary particles were not heavily agglomerated. It was also confirmed by SEM micrographs (Fig. 3a) that the synthesized powder was an irregular aggregates of nanometer particles. According to Park et al. [22], agglomeration of the precipitates is influenced by dielectric constant of the reaction medium. The lower the dielectric constant, the higher the degree of agglomeration. Since, 1,4-butanediol has quite high dielectric constant ($\varepsilon = 32$ at 25 °C [23]), the repulsive force between anatase particles formed in this reaction medium is more pronounced than the attraction force, resulting in low degree of agglomeration.

After calcination at 500 °C, the calcined powder was still in anatase phase, as previously proved that anatase synthesized by this method is thermally stable [21]. Nevertheless, the crystallite size of titania increased due to crystal growth. Agglomeration of primary particles was also observed, according to the fact that the BET surface area was notably decreased. Despite of the smaller surface area, calcined titania has shown higher photocatalytic activity than as-synthesized titania. This is due to the fact that the crystallinity of titania was improved by calcination and the crystallinity predominantly influenced the activity rather than surface area [24].

3.2. Photodegradation of diuron

It has been reported that titania synthesized by the thermal decomposition of titanium alkoxide in organic solvent has high activity in photocatalytic decomposition of various compounds [20]. In this work, titania synthesized by this method was employed as catalyst in the photodegradation of diuron, which is chemically stable pollutant. Since, the photocatalytic activity depends upon the conditions of the reaction, such as temperature, light intensity, initial concentration of the compound to be degraded and amount of catalyst used, it is difficult to directly compare the results obtained in this work to those reported in literatures. Therefore, in order to investigate activity of the in-house synthesized catalyst, the results were compared to that of the reference catalyst (JRC-TIO-1) from the Catalysis Society of Japan. It should be noted that mass of the reference catalyst used was the same as the mass of the in-house synthesized catalyst.

Table 1
Crystallite size and surface area of the synthesized products

	Crystallite size[a], d (nm)	S_{BET} (m^2/g)	S_{XRD} (m^2/g)
Synthesized titania			
Before calcination	13	113	120
After calcination	15	68	103
Reference titania	9	53	174

[a] Crystallite size calculated from XRD peak broadening.

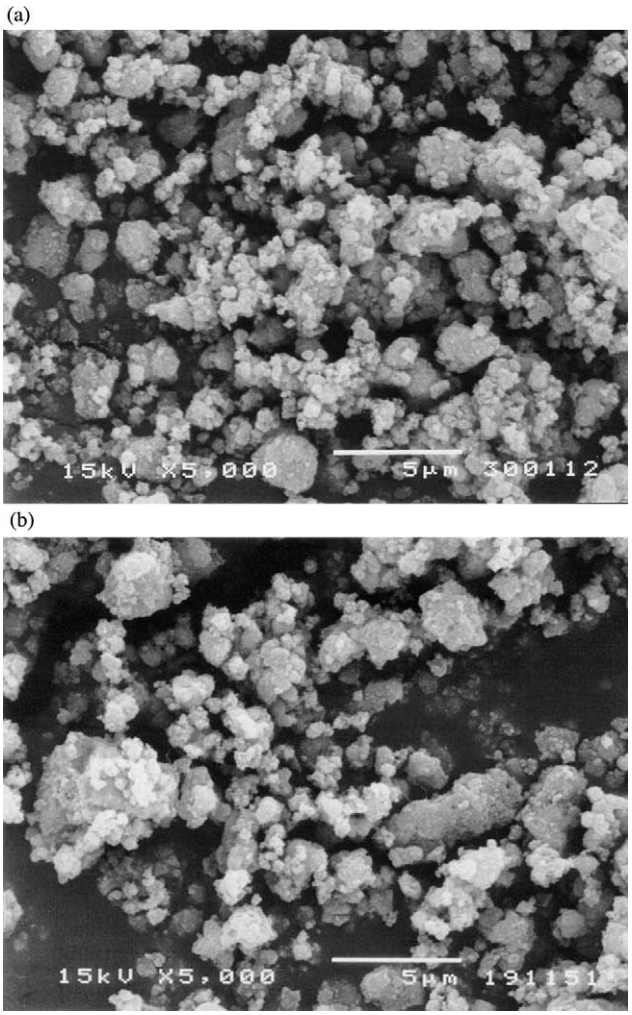

Fig. 3. SEM micrographs of synthesized titania: (a) before calcination, (b) after calcination.

Fig. 4 shows the disappearance of diuron by photocatalytic degradation using the synthesized titania or reference titania as catalyst. It should be noted that C is the concentration of diuron at time t, while C_0 is the initial diuron concentration. The results shown in Fig. 4a indicate

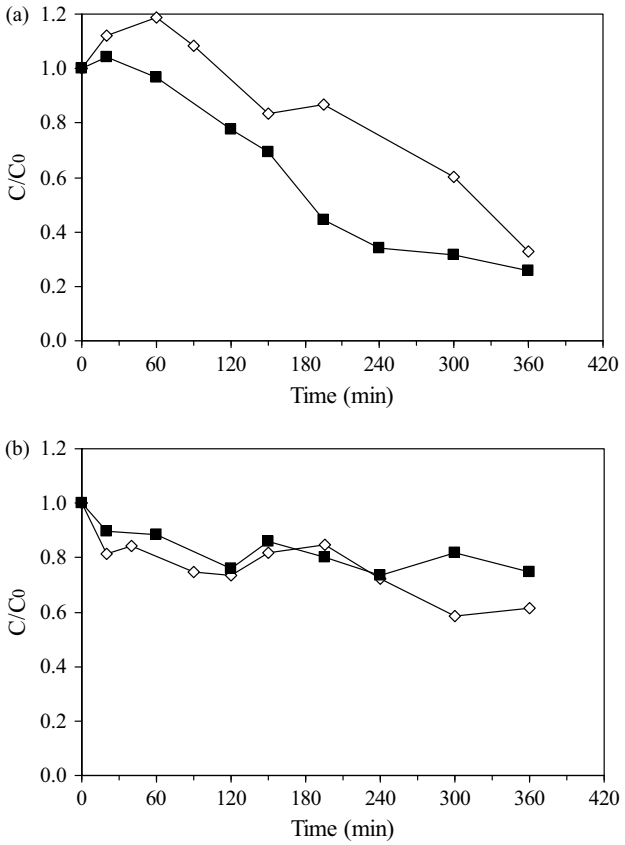

Fig. 4. Results for photocatalytic degradation of 1 ppm diuron aqueous solution: (a) in oxygen saturated solution, (b) in nitrogen-purged solution; (■) synthesized titania, (◇) reference titania.

that although both catalysts yielded approximately the same degradation after the reaction time of 6 h, the synthesized titania showed almost twice as much in the initial degradation rate than the reference catalyst. The amount of diuron was reduced to 30% of its initial value within 4 h of the reaction using the synthesized catalyst, while almost 6 h was required for the reference catalyst.

It has been recognized that the efficiency of titania in photocatalytic reaction is influenced by many factors such as crystallinity of the anatase phase [9], particle size [11] and surface area [11]. Since, the synthesized and reference titania are both anatase with roughly same particle size and surface area, the main factor accountable for the enhanced activity of the synthesized titania is its crystallinity. Although there has been no consensus on the detailed mechanism of the photocatalytic reaction on titania, it is generally agreed that the reaction involves generation of electron-hole pairs upon illumination of UV light on titania. The photogenerated holes can be subsequently scavenged by oxidizing species such as H_2O or OH^- and result in highly reactive hydroxyl radicals, which are the key for decomposition of most organic contaminants. Therefore, the separation of the photogenerated electron-hole pairs is considered to have a predominant role in photocatalytic reaction. The longer the separation period, the higher the activity. Crystallinity, including quality and quantity of both bulk and surface crystal defects, is one factor that affects the electron-hole separation [25]. It has been reported that negligible photocatalytic activity of amorphous titania is attributable to the facilitated recombination of photoexcited electrons and holes in the amorphous structure. Therefore, the result in Fig. 4a suggests that titania synthesized by thermal decomposition of TNB in 1,4-butanediol has structure with high crystallinity that prevents electron-hole recombination. This result supports the findings in our previous work that titania synthesized by this method was formed via crystallization pathway [21].

When all oxygen dissolved in the solution was purged by thoroughly bubbling with nitrogen gas, the conversion of diuron photodegradation dramatically decreased. As shown in Fig. 4(b), only about 30% of diuron was degraded within 6 h of the reaction with either the synthesized or the reference catalyst. This is in agreement with the generally accepted mechanism of the photocatalytic reaction that the presence of oxygen as an electron scavenger in the system is required for the course of the reaction [26–28]. Without electron scavenger, the electron-hole recombination spontaneously took place on the surface of titania. The enhanced effect from crystallinity of the synthesized titania was therefore compromised and the progress of the photocatalytic reactions from both catalysts were roughly the same. However, regardless of the depletion of dissolved oxygen in the solution, the reaction still slowly progressed. This was expected to be the results from chlorine radicals produced from diuron degradation. Several studies involving photocatalytic decomposition of chlorinated organic materials have proposed that chlorine radicals may be generated during photocatalysis [29] and these radicals participate in radical chain reactions [30–32].

Further, investigations on the enhanced activity of the synthesized titania were conducted by using solar irradiation, which had much higher light intensity than UV lamps. It should be noted that the concentration of

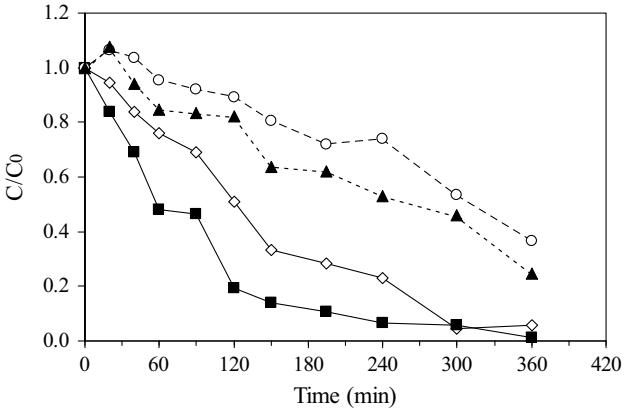

Fig. 5. Results for photocatalytic degradation of 10 ppm diuron aqueous solution: (- - -) using UV lamps, (—) using solar radiation; (■), (▲) synthesized titania, (◇), (○) reference titania.

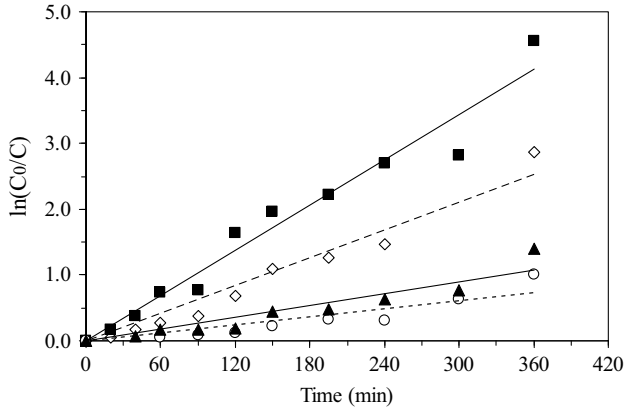

Fig. 6. First-order linear transforms of the degradation of 10 ppm diuron aqueous solution: (- - -) using UV lamps, (—) using solar radiation; (■), (▲) synthesized titania, (◇), (○) reference titania.

diuron employed was increased to 10 ppm in order to investigate the effect of the initial concentration as well. Fig. 5 shows the results comparing the photodegradation using sunlight to that using UV lamps. Furthermore, since rates of photooxidation of various organic contaminants over illuminated titania have been suggested to follow the Langmuir–Hinshelwood kinetics model [27,33,34], which can be simplified to the apparent first-order kinetics at low concentration, the plot of $\ln(C_0/C)$ versus time was expected to be a straight line with the slope equal to the apparent rate constant, k_{app}, of the degradation. The first-order linear transforms of the results shown in Fig. 5 are given in Fig. 6 and the rate constants are reported in Table 2.

Regarding the effect of diuron concentration, it was found that the degradation rate under UV light shown in Fig. 5 ($C_0 = 10$ ppm) was only slightly less than that was given in Fig. 4 ($C_0 = 1$ ppm). This is in general agreement with the pseudo first-order nature, according to the Langmuir–Hinshelwood kinetics, of the photooxidation on titania.

It can be seen from Figs. 5 and 6 that titania synthesized from thermal decomposition of titanium alkoxide has higher photocatalytic activity than the reference catalyst, especially under solar irradiation. Although it was not surprise to observe higher degradation rate under higher light intensity, it was particularly interesting to find that the enhancement in the activity from the synthesized titania increased with an increase in light intensity. According to Table 2, the reaction rate constant obtained from the synthesized titania was roughly 45% higher than that of the reference titania, when UV lamps were used. On the other hand, the rate from the synthesized titania was about 60% higher, under solar irradiation.

Table 2
Rate constants and half-life of the photocatalytic degradation reaction of diuron

	k_{app} (min^{-1})	$t_{1/2}$ (min)
Degradation using UV lamps		
Synthesized titania	3.003×10^{-3}	230.8
Reference titania	2.042×10^{-3}	339.5
Degradation using solar irradiation		
Synthesized titania	1.145×10^{-2}	60.5
Reference titania	7.027×10^{-3}	98.6

In general, under higher light intensity, more photo-electron-hole pairs are generated. However, it has been reported that a rate of the electron-hole recombination increases with increasing light intensity more progressively than the rates of charge transfer reaction [35]. Therefore, titania with high crystallinity, which prolongs the separation lifetime of the photogenerated electron-hole pairs, would utilize these greater amount of photoexcited electrons and holes with higher efficiency. Consequently, the enhancement in the photocatalytic activity under high light intensity is more pronounced than that from titania with lower crystallinity. This feature supports the aforementioned discussion that thermal decomposition of titanium alkoxide resulted in anatase titania with much higher crystallinity than the conventional preparation techniques.

Results discussed above have demonstrated that titania synthesized by thermal decomposition of TNB in 1,4-butanediol is potentially applicable for the photodegradation of diuron. However, the operating conditions for photocatalytic reaction in this work have not been optimized. Further, investigation on effects of degradation parameters on the degradation efficiency as well as the intermediates resulted from diuron degradation will be discussed in our next paper.

4. Conclusion

Nanocrystalline anatase titania can be prepared via thermal decomposition of TNB in 1,4-butanediol. The synthesized titania has shown higher photocatalytic activity comparing to the reference catalyst. It is suggested that the enhanced activity is resulted from high crystallinity of the synthesized powder, which consequently reduces the recombination of photogenerated electron-hole pairs. The synthesized titania also shows the potential for the degradation of chemically stable compound such as diuron. Nevertheless, conditions for photodecomposition need to be optimized.

Acknowledgements

The author would like to thank the Thailand Research Fund (TRF) and the Thailand-Japan Technology Transfer Project (TJTTP) for their financial support.

References

[1] K.E. Coulter, A.G. Sault, Effects of activation on the surface-properties of silica-supported cobalt catalysts, Journal of Catalysis 154 (1995) 56–64.

[2] T. Wakanabe, A. Kitamura, E. Kojima, C. Nakayama, K. Hashimoto, A. Fuijishima, in: D.E. Olis, H. Al-Ekabi (Eds.), Photocatalytic Purification and Treatment of Water and Air, Elsevier, Amsterdam, 1993, p. 747.

[3] A.M. Tonejc, M. Goti, B. Grzeta, S. Music, S. Popovi, R. Trojko, A. Turkovi, I. MuSevic, Transmission electron microscopy studies of nanophase TiO_2, Materials Science and Engineering B-Solid State Materials for Advanced Technology 40 (1996) 177–184.

[4] E. Traversa, G. Gnappi, A. Montenero, G. Gusmano, Ceramic thin films by sol–gel processing as novel materials for integrated humidity sensors, Sensors and Actuators B-Chemical 31 (1996) 59–70.

[5] B. Ohtani, S. Nishimoto, Effect of surface adsorptions of aliphatic-alcohols and silver ion on the photocatalytic activity of TiO_2 suspended in aqueous-solutions, Journal of Physical Chemistry 97 (1993) 920–926.

[6] B. O'Regan, M. Gratzel, A low-cost, high-efficiency solar cell based on dye-sensitized colloidal TiO_2 films, Nature 353 (1991) 737.

[7] Y.J. Liu, R.O. Claus, Blue light emitting nanosized TiO_2 colloids, Journal of the American Chemical Society 119 (1997) 5273–5274.

[8] S. Nishimoto, B. Ohtani, H. Kajiwara, T. Kagiya, Correlation of the crystal structure of titanium dioxide prepared from titanium tetra-2-propoxide with the photocatalytic activity for redox reactions in aqueous propan-2-ol and silver salt solutions, Journal of the Chemical Society-Faraday Transactions 1 (81) (1985) 61–68.

[9] M.A. Fox, M.T. Dulay, Heterogeneous photocatalysis, Chemical Reviews 93 (1993) 341–357.

[10] K. Tanaka, T. Hisanaga, A.P. Rivera, in: D.F. Ollis, H. Al-Ekabi (Eds.), Photocatalytic Purification and Treatment of Water and Air, Elsevier, Amsterdam, 1993, p. 169.

[11] N.P. Xu, Z.F. Shi, Y.Q. Fan, J.H. Dong, J. Shi, M.Z.C. Hu, Effects of particle size of TiO_2 on photocatalytic degradation of methylene blue in aqueous suspensions, Industrial and Engineering Chemistry Research 38 (1999) 373–379.

[12] T. Sato, Y. Yamamoto, Y. Fujishiro, S. Uchida, Intercalation of iron oxide in layered $H_2Ti_4O_9$ and $H_4Nb_6O_{17}$: visible-light induced photocatalytic properties, Journal of the Chemical Society-Faraday Transactions 92 (1996) 5089–5092.

[13] S. Uchida, Y. Yamamoto, Y. Fujishiro, A. Watanabe, O. Ito, T. Sato, Intercalation of titanium oxide in layered $H_2Ti_4O_9$ and $H_4Nb_6O_{17}$ and photocatalytic water cleavage with $H_2Ti_4O_9$/(TiO_2, Pt) and $H_4Nb_6O_{17}$/(TiO_2, Pt) nanocomposites, Journal of the Chemical Society-Faraday Transactions 93 (1997) 3229–3234.

[14] M. Inoue, Y. Kondo, T. Inui, An ethylene glycol derivative of boehmite, Inorganic Chemistry 27 (1988) 215–221.

[15] M. Inoue, H. Kominami, T. Inui, Thermal transformation of chi-alumina formed by thermal decomposition of aluminum alkoxide in organic media, Journal of the American Ceramic Society 75 (1992) 2597–2598.

[16] M. Inoue, H. Kominami, T. Inui, Novel synthetic method for the catalytic use of thermally stable zirconia—thermal decomposition of zirconium alkoxides in organic media, Applied Catalysis A-General 97 (1993) L25–L30.

[17] H. Kominami, J. Kato, S. Murakami, Y. Kera, M. Inoue, T. Inui, B. Ohtani, Synthesis of titanium (IV) oxide of ultra-high photocatalytic activity: high-temperature hydrolysis of titanium alkoxides with water liberated homogeneously from solvent alcohols, Journal of Molecular Catalysis A-Chemical 144 (1999) 165–171.

[18] S. Kongwudthiti, P. Praserthdam, P. Silveston, M. Inoue, Influence of synthesis conditions on the preparation of zirconia powder by the glycothermal method, Ceramics International 29 (2003) 807–814.

[19] O. Mekasuwandumrong, P.L. Silveston, P. Praserthdam, M. Inoue, V. Pavarajarn, W. Tanakulrungsank, Synthesis of thermally stable micro spherical chi-alumina by thermal decomposition of aluminum isopropoxide in mineral oil, Inorganic Chemistry Communications 6 (2003) 930–934.

[20] H. Kominami, J. Kato, Y. Takada, Y. Doushi, B. Ohtani, S. Nishimoto, M. Inoue, T. Inui, Y. Kera, Novel synthesis of microcrystalline titanium (IV) oxide having high thermal stability and ultra-high photocatalytic activity: thermal decomposition of titanium (IV) alkoxide in organic solvents, Catalysis Letters 46 (1997) 235–240.

[21] W. Payakgul, O. Mekasuwandumrong, V. Pavarajarn, P. Praserthdam, Effects of reaction medium on the synthesis of TiO_2 nanocrystals by thermal decomposition of titanium (IV) *n*-butoxide, Ceramics International 31 (2005) 391–397.

[22] H.K. Park, D.K. Kim, C.H. Kim, Effect of solvent on titania particle formation and morphology in thermal hydrolysis of $TiCl_4$, Journal of the American Ceramic Society 80 (1997) 743–749.

[23] J.A. Dean, Lange's Handbook of Chemistry, McGraw-Hill, New York, 1999.

[24] H. Kominami, S. Murakami, Y. Kera, B. Ohtani, Titanium (IV) oxide photocatalyst of ultra-high activity: a new preparation process allowing compatibility of high adsorptivity and low electron-hole recombination probability, Catalysis Letters 56 (1998) 125–129.

[25] S.J. Tsai, S. Cheng, Effect of TiO_2 crystalline structure in photocatalytic degradation of phenolic contaminants, Catalysis Today 33 (1997) 227–237.

[26] C. Kormann, D.W. Bahnemann, M.R. Hoffmann, Photocatalytic production of hydrogen peroxides and organic peroxides in aqueous suspensions of titanium dioxide, zinc oxide, and desert sand, Environmental Science & Technology 22 (1988) 798–806.

[27] A. Houas, H. Lachheb, M. Ksibi, E. Elaloui, C. Guillard, J.M. Herrmann, Photocatalytic degradation pathway of methylene blue in water, Applied Catalysis B-Environmental 31 (2001) 145–157.

[28] H.-S. Son, S.-J. Lee, I.-H. Cho, K.-D. Zoh, Kinetics and mechanism of TNT degradation in TiO_2 photocatalysis, Chemosphere 57 (2004) 309–317.

[29] M.R. Nimlos, W.A. Jacoby, D.M. Blake, T.A. Milne, Direct mass spectrometric studies of the destruction of hazardous wastes. 2. Gas-phase photocatalytic oxidation of trichloroethylene over TiO_2: products and mechanisms, Environmental Science & Technology 27 (1993) 732–740.

[30] Y. Luo, D.F. Ollis, Heterogeneous photocatalytic oxidation of trichloroethylene and toluene mixtures in air: kinetic promotion and inhibition, time-dependent catalyst activity, Journal of Catalysis 163 (1996) 1–11.

[31] O. dHennezel, D.F. Ollis, Trichloroethylene-promoted photocatalytic oxidation of air contaminants, Journal of Catalysis 167 (1997) 118–126.

[32] M. Lewandowski, D.F. Ollis, Halide acid pretreatments of photo-catalysts for oxidation of aromatic air contaminants: rate enhance-ment, rate inhibition, and a thermodynamic rationale, Journal of Catalysis 217 (2003) 38–46.

[33] W.Z. Tang, H. An, Photocatalytic degradation kinetics and mechan-ism of acid-blue-40 by TiO_2/UV in aqueous-solution, Chemosphere 31 (1995) 4171–4183.

[34] I.K. Konstantinou, V.A. Sakkas, T.A. Albanis, Photocatalytic degradation of propachlor in aqueous TiO_2 suspensions. Determi-nation of the reaction pathway and identification of intermediate products by various analytical methods, Water Research 36 (2002) 2733–2742.

[35] M.R. Hoffmann, S.T. Martin, W.Y. Choi, D.W. Bahnemann, Environmental applications of semiconductor photocatalysis, Chemical Reviews 95 (1995) 69–96.

Available online at www.sciencedirect.com
SCIENCE DIRECT
Materials Chemistry and Physics 97 (2006) 343–350
MATERIALS CHEMISTRY AND PHYSICS
www.elsevier.com/locate/matchemphys

Catalytic behaviors of mixed TiO_2-SiO_2-supported cobalt Fischer–Tropsch catalysts for carbon monoxide hydrogenation

Bunjerd Jongsomjit*, Tipnapa Wongsalee, Piyasan Praserthdam

Center of Excellence on Catalysis and Catalytic Reaction Engineering, Department of Chemical Engineering, Faculty of Engineering, Chulalongkorn University, Bangkok 10330, Thailand

Received 11 April 2005; received in revised form 7 July 2005; accepted 9 August 2005

Abstract

In the present study, the catalytic behaviors of mixed TiO_2-SiO_2-supported cobalt (Co) Fischer–Tropsch (FT) catalysts via carbon monoxide (CO) hydrogenation were investigated. The various weight ratios of TiO_2/SiO_2 were prepared, then consequently impregnated with the cobalt precursor. After calcination, the various samples were characterized using XRD, Raman spectroscopy, scanning electron microscopy/energy dispersive X-ray (SEM/EDX), transmission electron microscopy (TEM), temperature-programmed reduction (TPR), and H_2 chemisorption. The characteristics of various samples were further discussed in more details. Based on the reaction study, it revealed that the presence of titania in the mixed supports resulted in decreased activities dramatically. However, longer chain hydrocarbons such as C_2–C_5 can be obtained substantially with increasing the amounts of titania in the mixed supports.

Keywords: Silica; Titania; Cobalt; Catalyst; CO hydrogenation

1. Introduction

It has been known that supported cobalt (Co) catalysts are preferred for Fischer–Tropsch (FT) synthesis because of their high activities during FT synthesis based on natural gas [1], high selectivity to linear long chain hydrocarbons and also low activities for the competitive water–gas shift (WGS) reaction [2,3]. Many inorganic supports such as SiO_2 [4–8], Al_2O_3 [9–14], TiO_2 [15–17] and zeolites [18] have been extensively studied for supported Co catalysts for years. It is known that in general, the catalytic properties depend on reaction conditions, catalyst compositions, metal dispersion, and types of inorganic supports used. Thus, changes the catalyst compositions and/or even though the compositions of supports used may lead to significantly enhance the catalytic properties as well.

The TiO_2-SiO_2 mixed oxide has been considered to be very attractive as catalysts and supports, which have brought much attention in recent years. It was reported that TiO_2-SiO_2 mixed materials have been used as catalysts and supports for various reactions [19]. However, the use of this mixed oxide support here with the cobalt catalyst has not been reported yet. This TiO_2-SiO_2 mixed oxide would lead to robust catalytic supports of cobalt catalyst for carbon monoxide (CO) hydrogenation reaction.

Therefore, the main objective of this present study was to investigate the catalytic behaviors of mixed TiO_2-SiO_2-supported cobalt Fischer–Tropsch catalyst via CO hydrogenation reaction. The ratios of TiO_2/SiO_2 used were varied. The mixed oxide supports and catalyst precursors were prepared, characterized and tested for CO hydrogenation. The role of titania in the mixed oxide supports on the catalytic behaviors was also further discussed.

2. Experimental

2.1. Material preparation

2.1.1. Preparation of TiO_2-SiO_2 mixed oxide support

TiO_2-SiO_2 mixed oxide supports [surface areas of $SiO_2 = 300\,m^2\,g^{-1}$ and $TiO_2 = 70\,m^2\,g^{-1}$ (anatase form)]

* Corresponding author. Tel.: +662 2186869; fax: +662 2186877.
E-mail address: bunjerd.j@chula.ac.th (B. Jongsomjit).

0254-0584/$ – see front matter © 2005 Elsevier B.V. All rights reserved.
doi:10.1016/j.matchemphys.2005.08.016

were prepared according to the method described by Conway et al. [20]. In particular, 1 g of TiO_2-SiO_2 mixed oxide support was physically mixed by dispersing in toluene (ca. 20 ml). The mixture was stirred for 30 min, filtered, and then dried under vacuum. The TiO_2/SiO_2 weight ratios were varied from 0/1, 2/8, 4/6, 6/4, 8/2, and 1/0. The mixed supports were calcined at 500 °C for 4 h.

2.1.2. Preparation of catalyst samples

A 20 wt.% of Co/TiO_2-SiO_2 mixed support was prepared by the incipient wetness impregnation. A designed amount of cobalt nitrate [$Co(NO_3)\cdot 6H_2O$] was dissolved in deionized water and then impregnated onto the mixed oxide supports obtained from Section 2.1.1. The catalyst precursor was dried at 110 °C for 12 h and calcined in air at 500 °C for 4 h.

2.2. Catalyst nomenclature

The nomenclature used for the catalyst samples in this study is following:

- Co_*a*/*b* refers to the cobalt catalyst on the TiO_2-SiO_2 mixed oxide support, where *a* is the weight ratio of TiO_2 and *b* the weight ratio of SiO_2

2.3. Catalyst characterization

2.3.1. X-ray diffraction

XRD was performed to determine the bulk crystalline phases of catalyst. It was conducted using a SIEMENS D-5000 X-ray diffractometer with Cu Kα (λ = 1.54439 Å). The spectra were scanned at a rate of 2.4 ° min^{-1} in the range $2\theta = 20$–80°.

2.3.2. Raman spectroscopy

The Raman spectra of the samples were collected by projecting a continuous wave laser of argon ion (Ar^+) green (514.532 nm) through the samples exposed to air at room temperature. A scanning range of 100–1000 cm^{-1} with a resolution of 2 cm^{-1} was applied. The data were analyzed using the Renishaw Windows-based Raman Environment (WiRE) software, which allows Raman spectra to be captured, calibrated, and analyzed using system 2000 functionality via Galactic GRAMS interface with global imaging capacity.

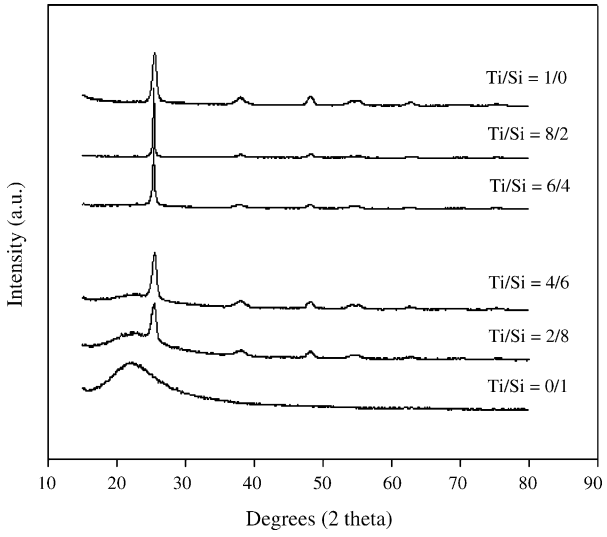

Fig. 1. XRD patterns for various ratios of TiO_2/SiO_2 mixed supports.

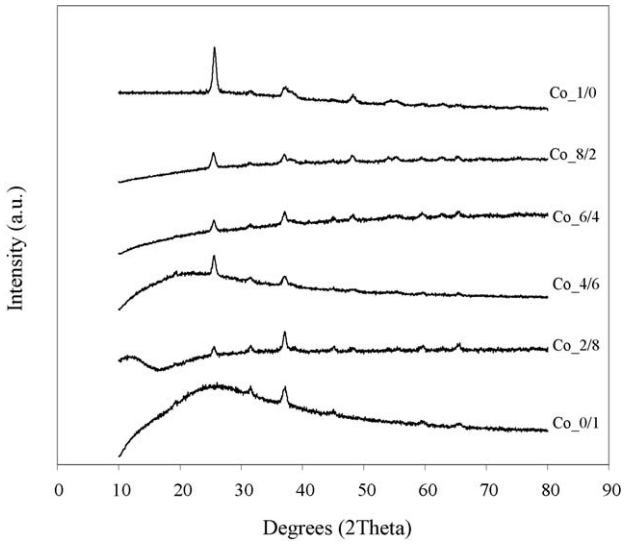

Fig. 2. XRD patterns for the various mixed TiO_2/SiO_2-supported cobalt catalysts after calcination.

2.3.3. Scanning electron microscopy (SEM) and energy dispersive X-ray (EDX) spectroscopy

SEM and EDX were used to determine the catalyst morphologies and elemental distribution throughout the catalyst granules, respectively. The SEM of JEOL mode JSM-5800LV was applied. EDX was performed using Link Isis series 300 program.

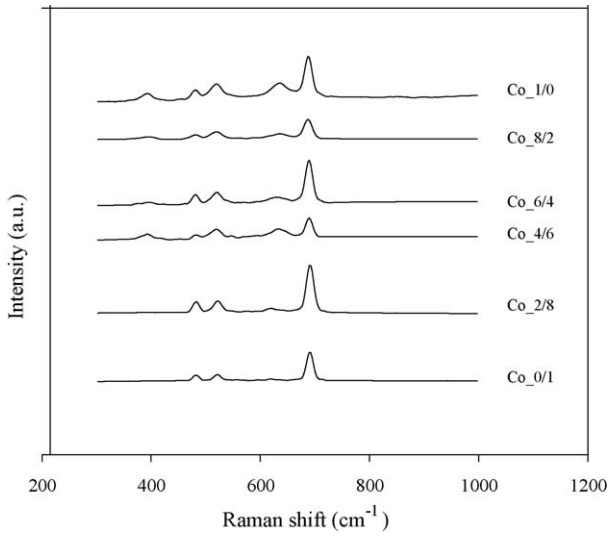

Fig. 3. Raman spectra for the various mixed TiO_2/SiO_2-supported cobalt catalysts after calcination.

2.3.4. Transmission electron microscopy (TEM)

The dispersion of cobalt oxide species on the various mixed oxide supports was determined using a JEOL-TEM 200CX transmission electron spectroscopy operated at 100 kV with 100k magnification.

2.3.5. Hydrogen chemisorption

Static H_2 chemisorption at 100 °C on the reduced cobalt catalysts was used to determine the number of reduced surface cobalt metal atoms. This is related to the overall activity of the catalysts during CO hydrogenation. Gas volumetric chemisorption at 100 °C was performed using the method described by Reuel and Bartholomew [21]. The experiment was performed in a Micromeritics ASAP 2010 using ASAP 2010C V3.00 software.

2.3.6. Temperature-programmed reduction (TPR)

TPR was used to determine the reduction behaviors and reducibilities of the samples. It was carried out using 50 mg of a sample and a temperature ramp from 35 to 800 °C at 5 °C min^{-1}. The carrier gas was 5% H_2 in Ar. A cold trap was placed before the detector to remove water produced during the reaction. A thermal conductivity detector (TCD) was used to determine the amount of H_2 consumed during TPR. The H_2 consumption was calibrated using TPR of Ag_2O at the same conditions [9,22–26].

2.4. Reaction

CO hydrogenation (H_2/CO = 10/1) was performed to determine the overall activity of the catalyst samples. Hydrogenation of CO was carried out at 220 °C and 1 atm. A flow rate of H_2/CO/He = 20/2/8 cc min^{-1} in a fixed-bed flow reactor under differential condition was used. A relatively high H_2/CO ratio was used to minimize deactivation due to carbon deposition during reaction. Typically, 20 mg of a catalyst sample was reduced in situ in flowing H_2 (30 cc min^{-1}) at 350 °C for 10 h prior to the reaction. Reactor effluent samples were taken at 1-h intervals and analyzed by GC. In all cases, steady-state was reached within 5 h.

3. Results and discussion

3.1. Characteristics of Co/TiO_2-SiO_2

The XRD patterns of mixed TiO_2-SiO_2 supports before impregnation with the cobalt precursor are shown in Fig. 1. It was observed that the pure silica exhibited a broad XRD peak assigning to the conventional amorphous silica. Similar to the pure silica, the XRD patterns of pure titania indicated only the characteristic peaks of anatase titania at 25° (major), 37°, 48°, 55°, 56°, 62°, 71°, and 75°. XRD patterns of the mixed oxide supports containing various ratios of titania and silica revealed the combination of titania and silica supports based on their contents. It can be seen that the intensity of XRD characteristic peaks for both supports was changed based on the ratios of titania and silica. After impregnation with the cobalt precursor and calcination, all samples of Co/TiO_2-SiO_2 catalyst were again identified using XRD. The XRD patterns of all calcined samples are shown in Fig. 2. After calcination, all samples exhibited XRD peaks,

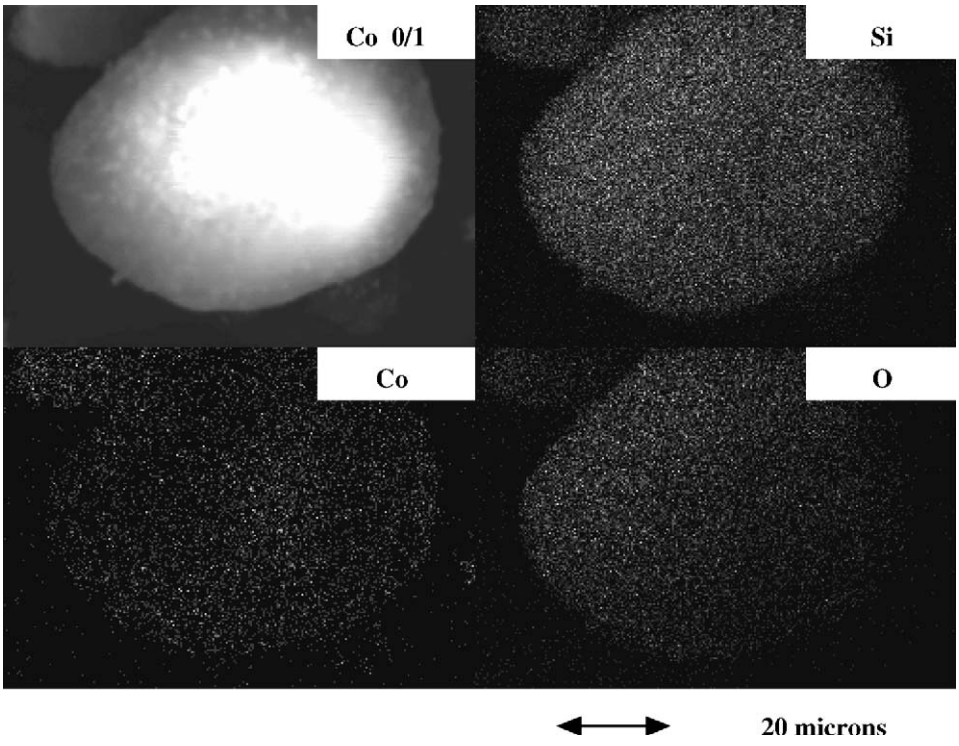

Fig. 4. SEM micrograph and EDX mapping of the calcined Co/SiO_2 catalyst.

which were identical with those for the corresponding mixed oxide supports used as seen in Fig. 1. This indicated that there was no further phase transformation from anatase to rutile occurred after calcination (at temperature ca. 500 °C for 4 h). The amorphous silica also exhibited good stability upon the same calcination process. Besides the corresponding mixed oxide supports detected, all calcined samples also exhibited weak XRD peaks at 31°, 36°, and 65°, which were assigned to the presence of Co_3O_4. Based on XRD results, it indicated that the presence of Co_3O_4 was apparently in the highly dispersed form. Raman spectroscopy is one of the most powerful techniques used to identify the metal oxide species present. It was found that the titania support exhibited the Raman bands at 640, 514 and 397 cm^{-1} for TiO_2 in its anatase form as seen from our previous work [27] whereas silica was the Raman insensitive upon the scanning range applied. The Raman spectra for all calcined samples as shown in Fig. 3 exhibited the Raman bands of the titania support as mentioned above with two shoulders at 690 and 480 cm^{-1}, assigned to Co_3O_4 [9,22,27] with corresponding to those with XRD.

SEM and EDX were also conducted in order to study the morphologies and elemental distribution of the samples, respectively. Apparently, SEM micrographs and EDX mapping exhibited similar trends of morphologies and elemental (Co, Si, Ti, and O) distributions. The typical SEM micrographs along with the EDX mapping (for Co, Si, and O) of Co/SiO_2 sample are illustrated in Fig. 4 indicating the external surface of the sample granule. It can be seen that the cobalt oxide species were well distributed (shown on EDX mapping) all over the sample granule. In order to determine the morphologies and elemental distributions of cobalt

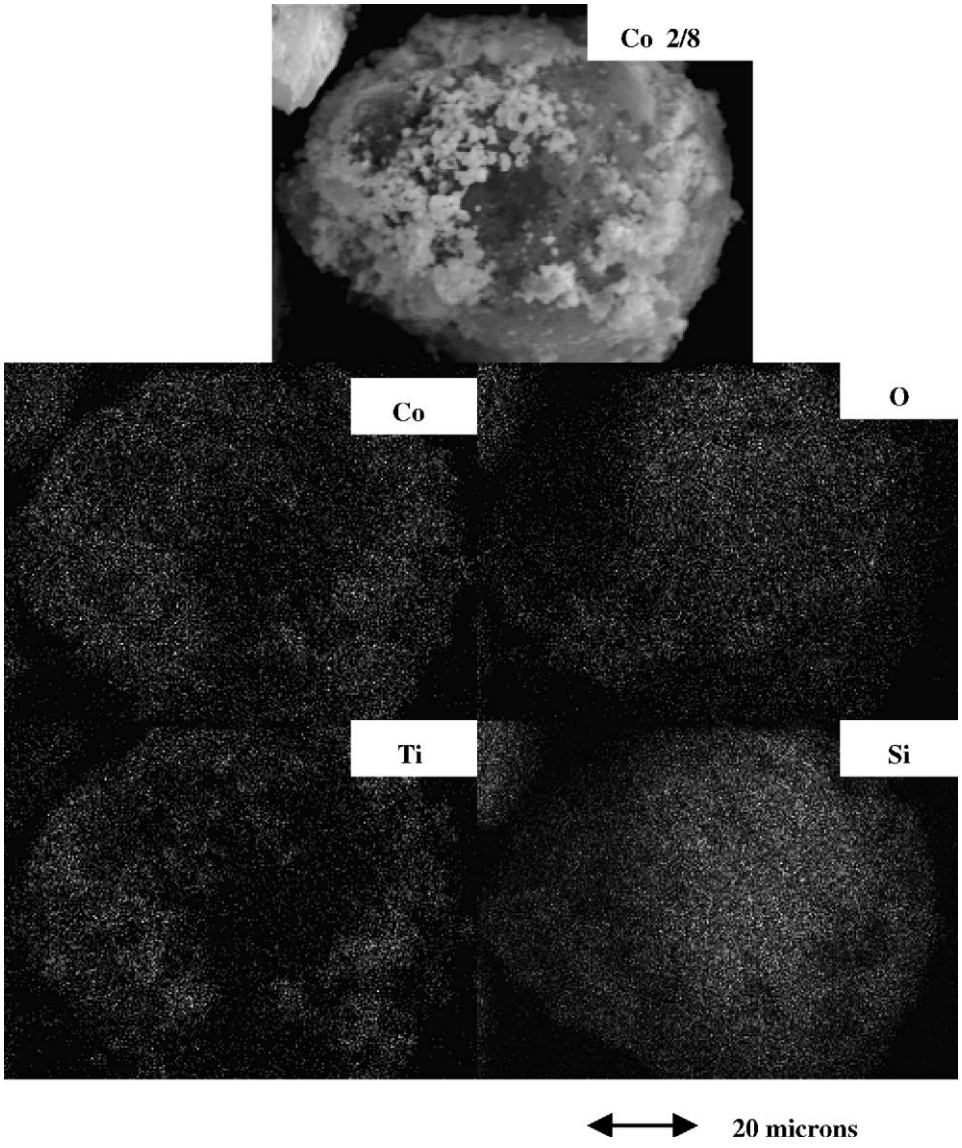

Fig. 5. SEM micrograph and EDX mapping of the calcined Co/TiO_2-SiO_2 (2/8) catalysts.

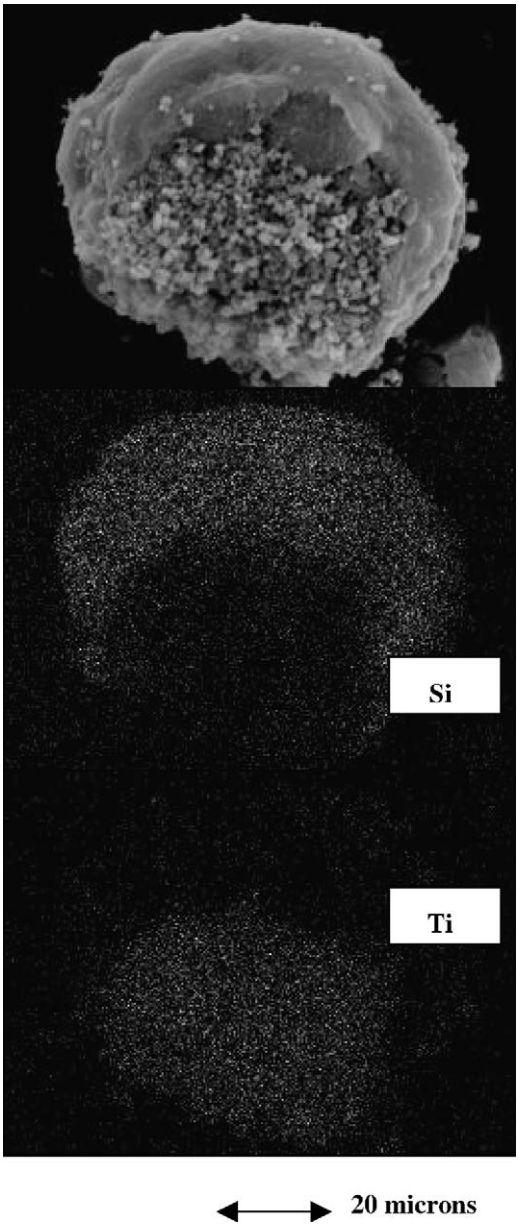

Fig. 6. A typical of SEM micrograph and EDX mapping of mixed TiO_2-SiO_2 support.

oxides on the mixed TiO_2-SiO_2 supports, the typical SEM micrographs along with the EDX mapping (for Co, Si, Ti, and O) are shown in Fig. 5, which is similar with those as seen in Fig. 4. However, an obvious charged surface under SEM electron bombarding is visible in Fig. 4. Besides the observation of well distribution for cobalt oxide species, it indicated that titania was apparently located on the outer surface of silica as shown in Fig. 6. The connectivity of Si–O–Ti can be confirmed by the IR spectroscopy indicating the IR bands at ca. 980 and 1100 cm^{-1} [28,29]. In order to determine the dispersion of cobalt oxide species on the various mixed oxide supports, a more powerful technique such as TEM was applied to all samples. The TEM micrographs for all samples are shown in Fig. 7. The dark spots represented cobalt oxide species or patches dispersing on the various mixed TiO_2-SiO_2 supports. It can be observed that a highly dispersed form of cobalt oxide species trended to be achieved with the presence of titania in the mixed oxide supports resulting in an appearance of smaller cobalt oxide patches. When combined the Raman spectroscopic results with those from TEM, it is likely that larger shoulders at 690 and 480 cm^{-1} would result in more dispersion of Co. It should be mentioned that although the more highly dispersed cobalt oxide patches with the presence of titania, their distributions seen by TEM were not as good as those seen in the pure silica support. On the other hand, the cobalt oxide patches present on the pure silica support exhibited better distribution, however, with lower degree of dispersion than any other samples. This can be attributed to higher surface areas of the silica support itself. It should be mentioned that high surface area of support could result in better distribution of Co, but somehow does not guarantee good dispersion (small Co patches). Besides, the highly dispersed form of cobalt oxide species could not guarantee the large number of reduced cobalt metal surface atoms, which is related to the overall activity of the catalyst. In addition, the highly dispersed form of cobalt oxide species, the interaction of those with the specified supports has to be essentially considered. Thus, temperature-programmed reduction on the calcined samples needs to be performed in order to give a better understanding according to such a reduction behavior. The TPR profiles for all samples are shown in Fig. 8. It was found that there was only one reduction peak, however, at different reduction temperatures for all calcined samples. The lowest reduction temperatures located at ca. 280–600 °C (maximum at 450 °C) was observed on the Co/SiO_2 sample. However, the reduction temperatures were found to dramatically shift to higher temperatures with increasing the amounts of titania present in the mixed oxide supports. Thus, the highest reduction temperatures located at ca. 370–650 °C (maximum at 550°C) can be observed for the Co/TiO_2 sample. The pronounced shift of reduction temperatures to higher ones found with the presence of titania can be attributed to the strong support interaction between the cobalt oxides and titania [30]. This was suggested that with the presence of titania it was more difficult for the cobalt oxide species to be reduced at the specified condition than those in silica itself. However, since the catalyst samples were reduced at different temperatures, it may not be useful to compare the reducibility of samples at this condition. Besides, the number of reduced Co metal surface atoms can be calculated directly from the H_2 chemisorption results, which is more acceptable since all catalyst samples are reduced at the standard reduction condition.

It is known that the active form of supported cobalt FTS catalysts is cobalt metal (Co^0). Thus, reduction of cobalt oxide species is essentially performed in order to transform cobalt oxide species obtained after calcination process into the active cobalt metal atoms for catalyzing the reac-

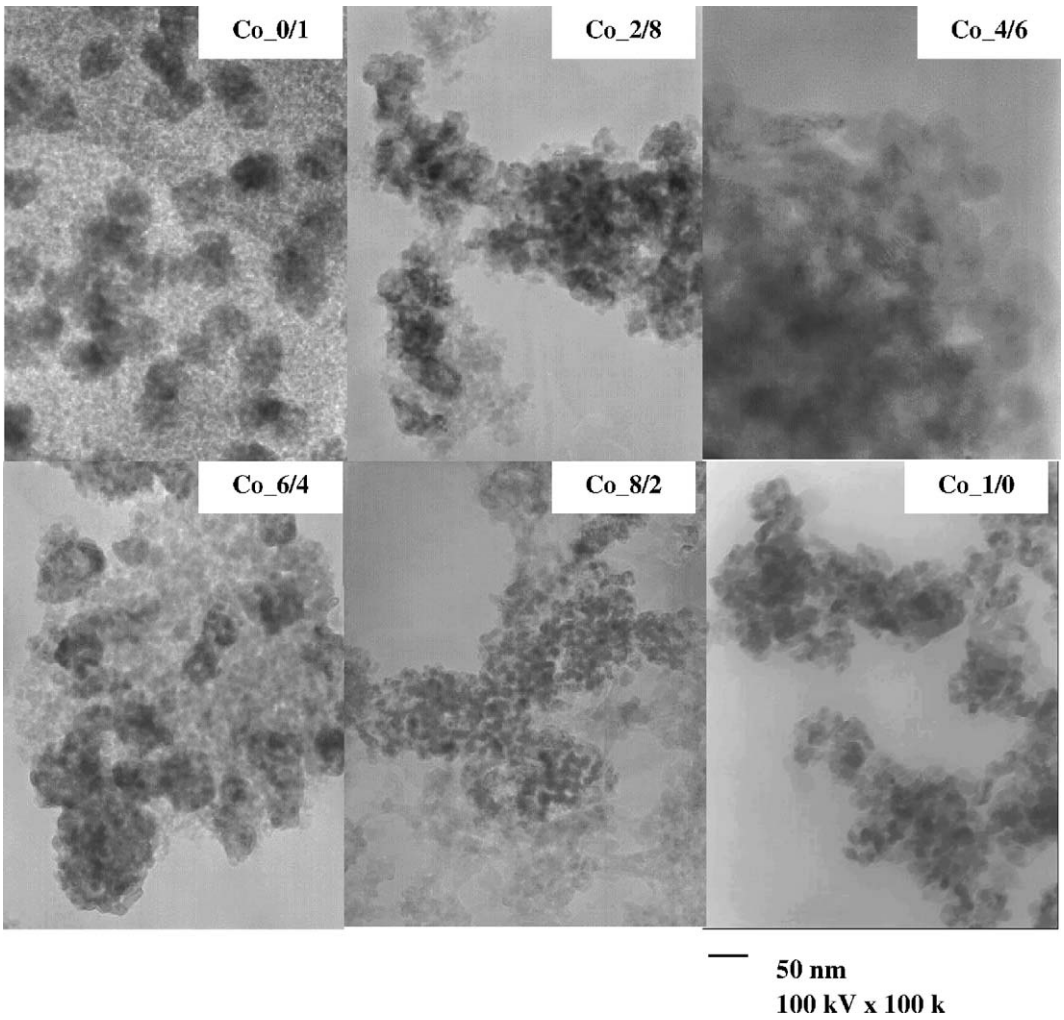

Fig. 7. TEM micrographs of the various mixed TiO_2/SiO_2-supported cobalt catalysts after calcinations.

tion. Therefore, the static H_2 chemisorption on the reduced cobalt samples was used to determine the number of reduced cobalt metal surface atoms. This is usually related to the overall activity of the catalyst during carbon monoxide hydrogenation. The resulted H_2 chemisorption for all samples are shown in Table 1. It revealed that the number of reduced cobalt metal surface atoms decreased with the amounts of titania present in the mixed oxide supports. These results were corresponding with those from the TPR as mentioned before.

3.2. Reaction study

In order to determine the catalytic behaviors of the cobalt catalyst on various mixed TiO_2-SiO_2 supports, CO hydrogenation (H_2/CO = 10/1) was performed to determine the

Table 1
Show the H_2 chemisorption, reaction rates, and product selectivity of various samples

Catalyst samples	H_2 Chemisorption (μmol g_{cat}^{-1})	Rate ($\times 10^2$ g CH_2 g_{cat}^{-1} h^{-1})[a]		Product selectivity[b] (%)	
		Initial[b]	SS[c]	CH_4	C_2–C_5
Co_0/1	11.11	38.9	34.3	99	1
Co_2/8	10.70	32.2	30.4	95	5
Co_4/6	1.85	14.2	10.0	87	13
Co_6/4	0.42	2.7	0.7	74	26
Co_1/0	0.22	1.4	0.8	68	32

[a] CO hydrogenation was carried out at 220 °C, 1 atm, and H_2/CO/He = 20/2/8.
[b] After 5 h of reaction.
[c] After 5 min of reaction.

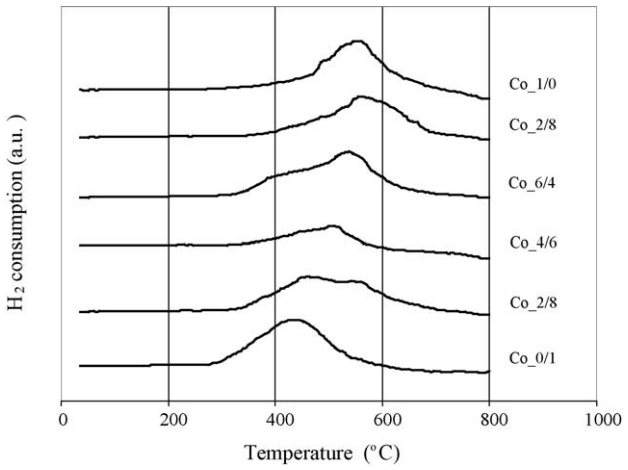

Fig. 8. TPR profiles of the various mixed TiO_2/SiO_2-supported cobalt catalysts after calcination.

overall activity and selectivity of the catalyst samples. Hydrogenation of CO was carried out at 220 °C and 1 atm. A flow rate of H_2/CO/He = 20/2/8 cc min^{-1} in a fixed-bed flow reactor under differential condition was used. In fact, a relatively high H_2/CO ratio was used to minimize deactivation due to carbon deposition during reaction. The resulted reaction study is also shown in Table 1. As expected, based on the H_2 chemisorption results, the overall activities for both initial and steady-state rates dramatically decreased with the amounts of titania present on the mixed oxide supports. This was basically due to the less number of reduced cobalt metal surface atoms with the presence of titania as seen by the H_2 chemisorption results along with higher surface area of silica as mentioned earlier. However, with some consideration on the product selectivity obtained, an interesting discovery can be observed in this present study. Considering the selectivity of product, it showed that the selectivity to methane essentially decreased with the amounts of titania in the supports. On the other hand, more amounts of longer chain hydrocarbons (C_2–C_5) can be obtained with the presence of titania in the mixed supports. It is known that CO hydrogenation is a kind of polymerization reactions where insertion of the $-CH_2-$ (methylene group) occurs through the active center. Thus, the product distribution strongly depends on the nature of active centers, rate of propagation, and rate of termination. Obviously, the termination of chain growth occurs and is recognized as the chain growth probability. Based on product selectivity found here, it can be concluded that the presence of titania in the mixed supports apparently inhibited the chain growth probability resulting in the observation of longer chain hydrocarbons even at the specified methanation condition. In order to study this effect in more details, the reaction intermediates at specified conditions must be further investigated with more powerful techniques such as the steady-state isotropic transient kinetic analysis (SSITKA) which has been successfully done by Goodwin and coworkers [5,6,8,9,31,32].

4. Summary

The present study showed impact of various mixed TiO_2-SiO_2-supported cobalt catalysts on their catalytic behaviors. It was found that both initial and steady-state rates during CO hydrogenation dramatically decreased with the amounts of titania present in the mixed supports. The decreased activities had to be attributed to the less number of reduced cobalt metal surface atoms for catalyzing the reaction. At the specified conditions, the selectivity of the longer chain hydrocarbons (C_2–C_5) was more pronounced with the presence of titania in the mixed supports. It can be concluded that the presence of titania apparently inhibited the chain growth probability during CO hydrogenation.

Acknowledgements

We gratefully acknowledge the financial support by the National Research Council of Thailand (NRCT), the Thailand Research Fund (TRF) and Thailand–Japan Technology Transfer Project (TJTTP-JBIC). We would like to thank Prof. James G. Goodwin Jr. at Clemson University for initiating this kind of project. We would like to extend our thanks to the National Metal and Materials Technology Center (MTECH) for Raman spectroscopy analysis.

References

[1] H.P. Wither Jr., K.F. Eliezer, J.W. Mechell, Ind. Eng. Chem. Res. 29 (1990) 1807.
[2] E. Iglesia, Appl. Catal. A 161 (1997) 59.
[3] R.C. Brady, R.J. Pettie, J. Am. Chem. Soc. 103 (1981) 1287.
[4] A. Martinez, C. Lopez, F. Marquez, I. Duaz, J. Catal. 220 (2003) 486.
[5] J. Panpranot, J.G. Goodwin Jr., A. Sayari, Catal. Today 77 (2002) 269.
[6] J. Panpranot, J.G. Goodwin Jr., A. Sayari, J. Catal. 211 (2002) 530.
[7] S.L. Sun, I. Isubaki, K. Fujimoto, Appl. Catal. A 202 (2000) 121.
[8] S. Ali, B. Chen, J.G. Goodwin Jr., J. Catal. 157 (1995) 35.
[9] B. Jongsomjit, J. Panpranot, J.G. Goodwin Jr., J. Catal. 215 (2003) 66.
[10] T. Das, G. Jacobs, P.M. Patterson, W.A. Conner, J.L. Li, B.H. Davis, Fuel 82 (2003) 805.
[11] G. Jacobs, P.M. Patterson, Y.Q. Zhang, T. Das, J.L. Li, B.H. Davis, Appl. Catal. A 233 (2002) 215.
[12] M. Rothaemel, K.F. Hanssen, E.A. Blekkan, D. Schanke, A. Holmen, Catal. Today 38 (1997) 79.
[13] V. Ragaini, R. Carli, C.L. Bianchi, D. Lorenzetti, G. Vergani, Appl. Catal. A 139 (1996) 17.
[14] V. Ragaini, R. Carli, C.L. Bianchi, D. Lorenzetti, G. Predieri, P. Moggi, Appl. Catal. A 139 (1996) 31.
[15] J.L. Li, G. Jacobs, T. Das, B.H. Davis, Appl. Catal. A 233 (2002) 255.
[16] G. Jacobs, T. Das, Y.Q. Zhang, J.L. Li, G. Racoillet, B.H. Davis, Appl. Catal. A 233 (2002) 263.
[17] J.L. Li, L.G. Xu, R. Keogh, B.H. Davis, Catal. Lett. 70 (2000) 127.
[18] X.H. Li, K. Asami, M.F. Luo, K. Michiki, N. Tsubaki, K. Fujimoto, Catal. Today 84 (2003) 59.

[19] X. Gao, I.E. Wachs, Catal. Today 51 (1999) 233.
[20] S.J. Conway, J.W. Falconer, C.H. Rochester, J. Chem. Soc., Faraday Trans. 185 (1989) 71.
[21] R.C. Reuel, C.H. Bartholomew, J. Catal. 85 (1984) 63.
[22] B. Jongsomjit, J. Panpranot, J.G. Goodwin Jr., J. Catal. 204 (2001) 98.
[23] B. Jongsomjit, J.G. Goodwin Jr., Catal. Today 77 (2002) 191.
[24] A. Kogelbauer, J.C. Weber, J.G. Goodwin Jr., Catal. Lett. 34 (1995) 269.
[25] Y. Zhang, D. Wei, S. Hammache, J.G. Goodwin Jr., J. Catal. 188 (1999) 281.
[26] B. Jongsomjit, C. Sakdamnuson, J.G. Goodwin Jr., P. Praserthdam, Catal. Lett. 94 (2004) 209.
[27] B. Jongsomjit, C. Sakdamnuson, P. Praserthdam, Mater. Chem. Phys. 89 (2005) 395.
[28] D.C.M. Dutoit, M. Schneider, J. Baiker, J. Catal. 153 (1995) 165.
[29] B. Jongsomjit, S. Ngamposri, P. Praserthdam, Catal. Lett. 100 (2005) 139.
[30] R. Riva, H. Miessuer, R. Vitali, G. Del Piero, Appl. Catal. A 196 (2000) 111.
[31] S. Vada, B. Chen, J.G. Goodwin Jr., J. Catal. 153 (1995) 224.
[32] S.H. Ali, J.G. Goodwin Jr., J. Catal. 176 (1998) 3.

Catalysis Letters Vol. 108, Nos. 1–2, April 2006 (© 2006)
DOI: 10.1007/s10562-006-0033-y

Effect of zirconia-modified titania consisting of different phases on characteristics and catalytic properties of Co/TiO_2 catalysts

Tipnapa Wongsalee, Bunjerd Jongsomjit*, and Piyasan Praserthdam

Center of Excellence on Catalysis and Catalytic Reaction Engineering, Department of Chemical Engineering, Faculty of Engineering, Chulalongkorn University, Bangkok 10330, Thailand

Received 8 November 2005; accepted 6 January 2006

The TiO_2 supports consisting of different phases were modified with ZrO_2 for TiO_2-supported Co catalysts. It showed that modification on the pure anatase TiO_2 resulted in decreased activities, but increased chain growth probability. In contrary, the modification on mixed phase TiO_2 resulted in increased activities without effects on selectivity.

KEY WORDS: cobalt catalyst; titania; support; zirconia modification; CO hydrogenation.

1. Introduction

In general, a supported catalyst usually consists of three components; (i) a catalytic phase, (ii) a promoter, and (iii) a support or carrier. As known, the catalytic properties apparently depend upon the components as mentioned above. The catalytic phase can be metals, metal oxides and so on. It can be used under a specified catalytic reaction. It is known that the catalytic performance is usually elevated using a promoter such as a noble metal. Besides the catalytic phase and promoter, it should be mentioned that a support could play a crucial role based on the catalytic performance. Basically, a support material acts as a carrier for the catalytic phase to be well dispersed on it. However, due to the supporting effects along with dispersion of the catalytic phase, the properties of a catalyst could be altered with the various supports used.

It is reported that many inorganic supports such as silica [1–4], alumina [5–9], titania [10–15], zirconia [16], and zeolites [17] have been extensively studied for years. During the past decades, titania-supported cobalt catalysts have been investigated by many authors, especially for the application of Fischer–Tropsch synthesis (FTS) in a continuously stirred tank reactor (CSTR) [10–12]. However, it should be noted that titania itself has different crystalline phases such as anatase, brookite and rutile phases. In our previous work, we reported that different crystalline phase compositions of titania could play important roles on the catalytic performance of titania-supported cobalt catalysts during CO hydrogenation [14,15,18]. In the present work, the modification of the titania support was extensively investigated. Since zirconia promotion appears to increase the rate of FTS on cobalt catalysts with silica support [19,20] and with alumina support [5], thus, it would be interesting to investigate the effect of zirconia modification on titania supports containing different phases.

In this study, a series of titania-supported cobalt catalysts was prepared with a range of zirconia concentrations in the titania supports. The titania supports used were in the pure anatase form and in the mixture of anatase and rutile phases. The catalysts were then characterized and tested for CO hydrogenation activity. The product selectivity was also further investigated.

*To whom correspondence should be addressed.
E-mail: bunjerd.j@chula.ac.th

2. Experimental

2.1. Materials

2.1.1. Zr-modified TiO_2 support

The Zr-modified titania supports were prepared by the impregnation method. There were two kinds of the titania supports used [(i) pure anatase phase and (ii) mixed anatase (81%) and rutile (19%) phases] from Ishihara Sangyo, Japan. First, Zr was impregnated into the support using a solution of zirconium (IV) *n*-propoxide (70 wt% in *n*-propanol, Alfa Aesar) to produce Zr-modified titania supports having 0.5, 1, and 5 wt% of ZrO_2. Second, the Zr-modified supports were calcined at 350 °C for 2 h (ramp rate 5 °C/min) prior to impregnation of cobalt.

2.1.2. Co/Zr-modified TiO_2 catalysts

Cobalt nitrate [$Co(NO_3)_2{\cdot}6H_2O$] was dissolved in deionized water and impregnated into the support as mentioned above to give a final catalyst with 20 wt% cobalt. The catalyst precursor was dried at 110 °C for 12 h and calcined in air at 500 °C for 4 h.

2.2. Catalyst nomenclature

The nomenclature used for the supports and catalyst samples in this study is as follows:

R0: TiO_2 support consisting of pure anatase phase
R19: TiO_2 support consisting of 81% anatase and 19% rutile phases
R0Z*i*: Zr-modified R0 with *i* wt% of ZrO_2
R19Z*i*: Zr-modified R19 with *i* wt% of ZrO_2
Co/support: supported cobalt catalyst on various supports as mentioned above

2.3. Characterization

2.3.1. BET surface area

BET surface area of the samples with various rutile: anatase ratios of titania was performed to determine if the total surface area changes. It was determined using N_2 adsorption at 77 K in a Micromeritics ASAP 2010.

2.3.2. X-ray diffraction

XRD was performed to determine the bulk crystalline phases of samples. It was conducted using a SIEMENS D-5000 X-ray diffractometer with CuK_α ($\lambda = 1.54439$ Å). The spectra were scanned at a rate of 2.4°/min in the range $2\theta = 20$–80°.

2.3.3. Temperature-programmed reduction

TPR was used to determine the reduction behaviors of the catalyst samples. It was carried out using 50 mg of a sample and a temperature ramp from 35 to 800 °C at 5 °C/min. The carrier gas was 5% H_2 in Ar. A cold trap was placed before the detector to remove water produced during the reaction.

2.3.4. Scanning electron microscopy and energy dispersive X-ray spectroscopy

SEM and EDX were used to determine the sample morphologies and elemental distribution throughout the sample granules, respectively. The SEM of JEOL model JSM-5800LV was applied. EDX was performed using Link Isis series 300 program.

2.3.5. Transmission electron microscopy (TEM)

The dispersion of cobalt oxide species on the titania supports were determined using a JEOL-TEM 200CX transmission electron spectroscopy operated at 200 kV with 200 k magnification.

2.3.6. Hydrogen chemisorption

Static H_2 chemisorption at 100 °C on the reduced samples was used to determine the number of reduced surface cobalt metal atoms. This is related to the overall activity of the samples during CO hydrogenation. Gas volumetric chemisorption at 100 °C was performed using the method described by Reuel and Bartholomew [21]. The experiment was performed in a Micromeritics ASAP 2010 using ASAP 2010C V3.00 software.

2.4. Reaction

CO hydrogenation (H_2/CO = 10/1) was performed to determine the overall activity and selectivity of the catalyst samples. It was carried out at 220 °C and 1 atm. A flow rate of H_2/CO/He = 20/2/8 cc/min in a fixed-bed flow reactor was used. A relatively high H_2/CO ratio was used to minimize deactivation due to carbon deposition during reaction. Typically, 20 mg of a catalyst sample was reduced in situ in flowing H_2 (30 cc/min) at 350 °C for 10 h prior to the reaction. Reactor effluent samples were taken at 1 h intervals and analyzed by GC. In all cases, steady-state was reached within 5 h. In fact, the reaction test for each sample was performed at least three times. The average point was reported.

3. Results and discussion

3.1. Characteristics

The BET surface areas of the modified supports and catalysts samples are shown in table 1. For the modified R0 (pure anatase) samples, the surface areas decreased from 70 to 47 m^2/g upon the amounts of zirconia loading. Based on the results of BET surface areas as shown in table 1, it showed that the surface area essentially slightly decreased with 0.5% Zr. The sintering was not the cause since the calcination temperature was only 350 °C. The decrease in surface area should be due to the pore blockage. The modified R19 (mixed phases) also showed decreases in surface areas from 49 to 33 m^2/g with zirconia modification. It can be observed that the surface areas of the catalyst samples on the various unmodified and modified supports slightly decreased with corresponding to the content of supports used. It should be noted that no significant changes in surface areas of samples were observed. After calcination, the various supports were characterized using XRD as shown in figure 1. For the R0 support, XRD peaks of the anatase phase of titania at 25°

Table 1
BET surface areas of various supports and catalyst samples

Supports	BET surface area (m^2/g)[a]	Catalyst samples	BET surface area (m^2/g)[a]
R0	70	Co/R0	52
R0Z0.5	55	Co/R0Z0.5	43
R0Z1	53	Co/R0Z1	42
R0Z5	47	Co/R0Z5	36
R19	49	Co/R19	34
R19Z0.5	38	Co/R19Z0.5	27
R19Z1	34	Co/R19Z1	25
R19Z5	33	Co/R19Z5	25

[a]Measurement error is ±5%.

2.2. Catalyst nomenclature

The nomenclature used for the supports and catalyst samples in this study is as follows:

R0: TiO_2 support consisting of pure anatase phase
R19: TiO_2 support consisting of 81% anatase and 19% rutile phases
R0Z*i*: Zr-modified R0 with *i* wt% of ZrO_2
R19Z*i*: Zr-modified R19 with *i* wt% of ZrO_2
Co/support: supported cobalt catalyst on various supports as mentioned above

2.3. Characterization

2.3.1. BET surface area

BET surface area of the samples with various rutile: anatase ratios of titania was performed to determine if the total surface area changes. It was determined using N_2 adsorption at 77 K in a Micromeritics ASAP 2010.

2.3.2. X-ray diffraction

XRD was performed to determine the bulk crystalline phases of samples. It was conducted using a SIEMENS D-5000 X-ray diffractometer with CuK_α ($\lambda = 1.54439$ Å). The spectra were scanned at a rate of 2.4°/min in the range $2\theta = 20$–80°.

2.3.3. Temperature-programmed reduction

TPR was used to determine the reduction behaviors of the catalyst samples. It was carried out using 50 mg of a sample and a temperature ramp from 35 to 800 °C at 5 °C/min. The carrier gas was 5% H_2 in Ar. A cold trap was placed before the detector to remove water produced during the reaction.

2.3.4. Scanning electron microscopy and energy dispersive X-ray spectroscopy

SEM and EDX were used to determine the sample morphologies and elemental distribution throughout the sample granules, respectively. The SEM of JEOL model JSM-5800LV was applied. EDX was performed using Link Isis series 300 program.

2.3.5. Transmission electron microscopy (TEM)

The dispersion of cobalt oxide species on the titania supports were determined using a JEOL-TEM 200CX transmission electron spectroscopy operated at 200 kV with 200 k magnification.

2.3.6. Hydrogen chemisorption

Static H_2 chemisorption at 100 °C on the reduced samples was used to determine the number of reduced surface cobalt metal atoms. This is related to the overall activity of the samples during CO hydrogenation. Gas volumetric chemisorption at 100 °C was performed using the method described by Reuel and Bartholomew [21]. The experiment was performed in a Micromeritics ASAP 2010 using ASAP 2010C V3.00 software.

2.4. Reaction

CO hydrogenation ($H_2/CO = 10/1$) was performed to determine the overall activity and selectivity of the catalyst samples. It was carried out at 220 °C and 1 atm. A flow rate of $H_2/CO/He = 20/2/8$ cc/min in a fixed-bed flow reactor was used. A relatively high H_2/CO ratio was used to minimize deactivation due to carbon deposition during reaction. Typically, 20 mg of a catalyst sample was reduced *in situ* in flowing H_2 (30 cc/min) at 350 °C for 10 h prior to the reaction. Reactor effluent samples were taken at 1 h intervals and analyzed by GC. In all cases, steady-state was reached within 5 h. In fact, the reaction test for each sample was performed at least three times. The average point was reported.

3. Results and discussion

3.1. Characteristics

The BET surface areas of the modified supports and catalysts samples are shown in table 1. For the modified R0 (pure anatase) samples, the surface areas decreased from 70 to 47 m^2/g upon the amounts of zirconia loading. Based on the results of BET surface areas as shown in table 1, it showed that the surface area essentially slightly decreased with 0.5% Zr. The sintering was not the cause since the calcination temperature was only 350 °C. The decrease in surface area should be due to the pore blockage. The modified R19 (mixed phases) also showed decreases in surface areas from 49 to 33 m^2/g with zirconia modification. It can be observed that the surface areas of the catalyst samples on the various unmodified and modified supports slightly decreased with corresponding to the content of supports used. It should be noted that no significant changes in surface areas of samples were observed. After calcination, the various supports were characterized using XRD as shown in figure 1. For the R0 support, XRD peaks of the anatase phase of titania at 25°

Table 1
BET surface areas of various supports and catalyst samples

Supports	BET surface area (m^2/g)[a]	Catalyst samples	BET surface area (m^2/g)[a]
R0	70	Co/R0	52
R0Z0.5	55	Co/R0Z0.5	43
R0Z1	53	Co/R0Z1	42
R0Z5	47	Co/R0Z5	36
R19	49	Co/R19	34
R19Z0.5	38	Co/R19Z0.5	27
R19Z1	34	Co/R19Z1	25
R19Z5	33	Co/R19Z5	25

[a]Measurement error is ± 5%.

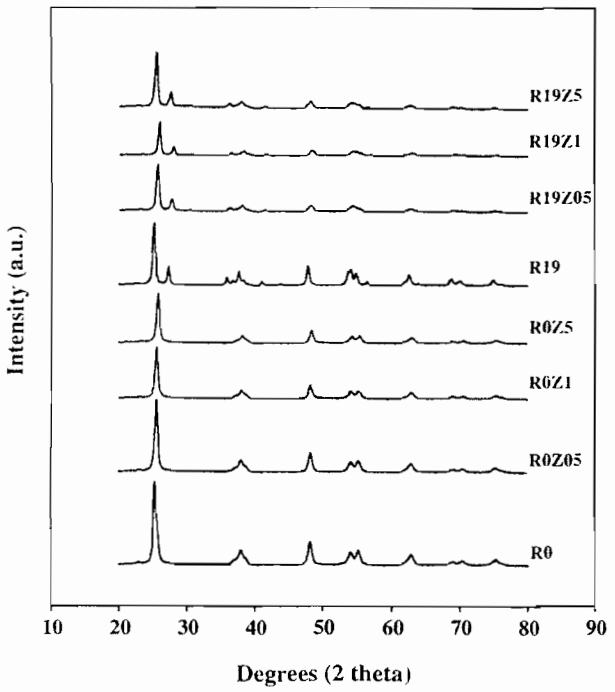

Figure 1. XRD patterns for different TiO_2 supports consisting of various amounts of ZrO_2 loading.

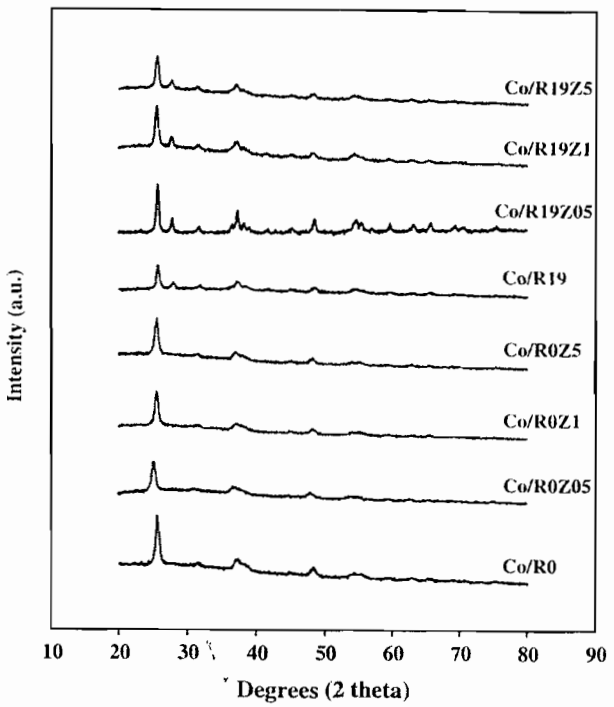

Figure 2. XRD patterns of Co/TiO_2 samples consisting of various amounts of ZrO_2 loading in TiO_2 supports.

(major), 37°, 48°, 55°, 56°, 62°, 71°, and 75° were evident. After the modification of R0 support, it was found that their characteristic peaks were still identical with those for the unmodified R0 support. This suggested that the zirconia was in the highly dispersed form. For the R19 support, it can be observed that besides the XRD peaks of pure anatase titania as mentioned before, the peaks at 28° (major), 36°, 42°, and 57° were detected. These peaks were assigned to the presence of rutile phase in the support along with the anatase phase. None of XRD peaks for zirconia was detected in the modified supports. After impregnation with the cobalt precursor and calcination, all catalyst samples were again identified using XRD. The XRD patterns of all calcined samples are shown in figure 2. It was observed that all calcined samples exhibited XRD peaks, which were identical with those for the corresponding modified supports as shown in figure 1. However, only weak intensity of XRD peak at 31° assigning to the presence of Co_3O_4 was detected. Therefore, based on the XRD results, it indicated that the presence of zirconia and cobalt oxide species were in the highly dispersed forms.

SEM and EDX were also conducted in order to study the morphologies and elemental distribution of the samples, respectively. In general, there was no significant change in morphologies and elemental distribution of all samples after calcination. The typical SEM micrograph and EDX mapping for Co/R19Z1 sample are illustrated in figure 3. Apparently, the Co oxide species exhibited well distribution on the surface of the support. In order to determine the dispersion of Co oxide species on the various modified supports, a more powerful technique such as TEM was applied to all samples. The TEM micrographs for Co/R0Z1, Co/R0Z5, Co/R19Z1, and Co/R19Z5 samples are shown in figure 4. The dark spots represented cobalt oxide species dispersing on the various modified supports after calcination of samples. The diameter of cobalt oxide particles was ca. 15, 16, 18, and 24 nm for Co/R0Z1, Co/R0Z5, Co/R19Z1, and Co/R19Z5 samples, respectively. Based on the TEM results, it indicated that the sizes of cobalt oxide species were slightly larger for those dispersing on the R19 supports than on the R0 supports as also reported in our previous work [14].

TPR was performed in order to determine the reduction behaviors of samples. The TPR profiles for all catalyst samples are shown in figure 5. The reduction temperatures for initial, final, and maximum temperatures are shown in table 2. It was found that there was only one reduction peak, however, at different reduction temperatures for all calcined samples. The one reduction peak can be assigned to the overlap of two step reduction of Co_3O_4 to CoO and then to Co metal [9,13]. Upon the TPR conditions, the two-step reduction may or may not be observed. Based on the TPR profiles, it indicated that for the zirconia-modified R0 supports, the reduction temperatures essentially shifted to the higher ones. Thus, zirconia modification of the R0 supports retarded the reduction of cobalt oxide species. Considering the zirconia modification of the R19 supports, it appeared that no effect on reduction behaviors of cobalt oxide species was found. However, it was confirmed that the